ISSN 0016-7029, Geochemistry International, 2008, Vol. 46, No. 12, pp. 1206–1227. © Pleiades Publishing, Ltd., 2008.
Original Russian Text © A.V. Dubinin, T.Yu. Uspenskaya, G.M. Gavrilenko, V.A. Rashidov, 2008, published in Geokhimiya, 2008, No. 12. pp. 1280–1303.

Geochemistry and Genesis of Fe–Mn Mineralization in Island Arcs in the West Pacific Ocean

A. V. Dubinin[a], T. Yu. Uspenskaya[a], G. M. Gavrilenko[b], and V. A. Rashidov[b]

[a] *Shirshov Institute of Oceanology, Russian Academy of Sciences, Nakhimovskii pr. 36, Moscow, 117997 Russia.*
[b] *Institute of Volcanology and Seismology, Far East Division, Russian Academy of Sciences, bul'v. Piipa 9, Petropavlosk-Kamchatskii, 683006 Russia.*
e-mail: dubinin@ocean.ru

Received September 7, 2007

Abstract—This paper presents materials on the chemical and mineralogical composition of Fe–Mn mineralization in island arcs (Kurile, Nampo, Mariana, New Britain, New Hebrides, and Kermadec) in the western part of the Pacific Ocean. The mineralization was proved to be of hydrothermal and/or hydrogenic genesis. The former is produced by hydrothermal Fe and Mn oxi-hydroxides that cement volcanic–terrigenous material in sediments. Some Fe oxi-hydroxides can be derived via the halmyrolysis of volcaniclastic material. Crusts of this stage are characterized by fairly low concentrations of trace and rare elements, and their REE composition is inherited from the volcanic–terrigenous material. The minerals of the Mn oxi-hydroxides are todorokite and "Ca-birnessite." The Mn/Fe ratio increases away from the discharge sites of the hydrothermal solutions.
The hydrogenic Fe–Mn crusts are characterized by high concentrations of trace and minor elements of both the Mn group (Co, Ni, Tl, and Mo) and the Fe group (REE, Y, and Th). The hydrogenic crusts consist of Fe-vernadite and Mn-feroxyhyte. Some of the hydrothermal crusts originally had a hydrothermal genesis. The first data were obtained on crust B30-72-10 from the Macauley Seamount in the Kermadec island arc, which contained anomalously high concentrations of Co (2587 ppm) and other Mn-related trace elements in the absence of hydrogeneous Fe oxi-hydroxides.

DOI: 10.1134/S0016702908120021

INTRODUCTION

Crusts and nodules of Fe and Mn oxi-hydroxides on the ocean floor continue to attract the interest of many researchers. Being good sortbents, Fe and Mn oxi-hydroxides are able to accumulate significant concentrations of rare and trace elements that may be economically important in the future.

Significant accumulations of rare and trace elements are contained only in pelagic crusts and nodules, which are dominated by hydrogenic and/or hydrogenic–diagenetic Fe and Mn oxides. Fe–Mn mineralization produced by the near-continent type of lithogenesis is poorer in trace elements, a feature believed to be indirectly related to higher (compared to those in pelagic environments) growth rates. The trace-element composition of Fe–Mn mineralization in oceans and seas depends (when all other conditions remain the same) on the Mn/Fe ratio. An increase in this ratio in pelagic nodules is explained by the different mobility of Mn^{2+} and Fe^{3+} in early diagenetic reactions, because Fe^{3+} cannot be reduced in the system nodule–host sediment with Mn^{4+} under equilibrium conditions. In the near-continent type of lithogenesis, reduced Mn passes into bottom waters at high fluxes of organic matter, and the sediments usually contain Fe-rich and Mn-poor oxi-hydroxide aggregates. In the course of normal sedimentation, the processes controlling the composition of Fe–Mn mineralization in oceans and seas are complicated by the effect of a hydrothermal source of material in spreading and subduction zones of lithospheric plates and in zones of within-plate volcanism. Hydrothermal solutions bring much reduced Fe and Mn into the bottom waters of oceans and seas. The bulk of the dissolved Fe^{2+} is oxidized within a few minutes after this [1], and, as a consequence, Fe and Mn become separated in the sedimentary process, because Mn can be transported for significant distances owing to its low oxidation rate [2]. As a result, discharge sites of hydrothermal solutions are often surrounded by Fe-rich (ocher) deposits or Mn-rich rapidly growing crusts if the mixing processes of the hydrothermal solution and seawater occur beneath the seafloor surface. Variations in the contribution of hydrothermal and hydrogenic material bring about variations in the composition of the Fe–Mn mineralization, which results in variations in both the Mn/Fe ratio and the composition and concentrations of trace elements. Significant fluxes of Fe and Mn of hydrothermal provenance form Fe–Mn mineralization with low concentrations of trace elements (for example, Co) [3].

Our research was focused on the study of the mineralogy and chemistry of Fe–Mn deposits at island arcs in the western part of the Pacific Ocean. Regional oceanic sedimentogenesis is complicated by both volcanic and related hydrothermal activity. Consequently, adjacent Fe–Mn deposits may significantly differ in composition and genesis. The aim of our research was to carry out a comparative study of Fe–Mn crusts at spatially separated discrete areas, from the Kurile island arc in the north to the Kermadec island arc in the south. Our study was conducted on 24 samples of Fe–Mn mineralization. One sample was taken from Ushishir volcano on a seamount of the Shokalsky Ridge, not far from Iturup Island, in the Kurile island arc; four samples are from various sites in the Nampo island arc; five were sampled at the slopes of Esmeralda submarine volcano at the Mariana island arc; six samples are from Matupi Harbor in the New Britain island arc; one sample was collected at Epi submarine volcano in the New Hebrides island arc; and five samples were dredged from a diversity of structures in the Kermadec island arc. We have also analyzed one sample from the Charlotte Bank in the South China Sea (Fig. 1). Our comparative study was carried out to determine the genesis of Fe–Mn deposits sampled not far from one another. The influence of material sources on their composition led to variations in their mineralogy and concentrations of trace elements.

MATERIALS AND METHODS

The materials for our research were obtained mostly from dredges lifted during cruises of the R/V *Vulkanolog* and R/V *Akademik Nesmeyanov*. The coordinates of the sampling sites and brief descriptions of the samples, including their numbers and sampling depths, are given in Table 1 and shown in Fig. 1. If the material of a sample looked megascopically homogeneous, material (<5 mm) was taken from the surface of the sample. If a crust had different upper and lower parts (crust B30-72-10), two samples (samples 1 and 2 in Table 2 and Fig. 2a) were collected. In the Matupi Harbor, New Britain Island, we examined Fe–Mn pipes though which hydrothermal solution flew. Upon closer examination it was revealed that the pipes are zonal, with their inner parts filled with sedimentary material (which likely filled the pipes after the hydrothermal activity terminated, and solutions ceased to flow along them) (Fig. 2b). One of our samples (sample H18-21) included a Fe-rich outer and a Mn-rich inner zone of the pipe and material that supposedly represented sediments from the harbor, which filled the pipe later (samples 1, 2, and 3, respectively, in Fig. 2b). The inner zone of the pipe was fairly thin (<1 mm) and differed from the outer Fe-rich zone (1–3 mm thick) in having a black color (Fig. 2b).

In preparation for their chemical analysis, air-dried samples of the Fe–Mn mineralization were crushed and powdered, and 30- to 50-mg samples were doubly treated by a mixture of concentrated HF, HNO_3, and $HClO_4$ in glass carbon crucibles at a temperature of 160–180°C until complete evaporation. Mn(IV) oxide that precipitated during the decomposition of the Fe–Mn minerals was reduced with 1 ml of 6 M HCl. Upon evaporation to dry salt, the samples were dissolved in 5 vol % solution of HNO_3 and were then analyzed for REE, Li, Be, Ga, Rb, Sr, Cd, Cs, Ba, Mo, W, Tl, Pb, Y, U, and Th by ICP-MS on a PlasmaQuad PQ2STE (Fisons Instruments) [4, 5]. Fe, Mn, Co, Ni, Cu, Zn, and Al were determined in the same samples by atomic absorption on Spectr AA220 (Varian). The analyses were accurate to at least 3%. Phosphorus was analyzed on a spectrophotometer by the color intensity of blue phosphorus–molybdenum–antimony complex. The precision of the analysis was 3%. The application accuracy of the analytical techniques was controlled by replicate analyses of the standards SDO-9 (red pelagic clay), SDO-5 (Fe–Mn nodule), and SDO-2 (volcanic–terrigenous ooze). Our data on the chemical composition of the Fe–Mn deposits are summarized in Table 2.

The mineralogy of the samples was identified by transmitted analytical electron microscopy (modification of electrons and energy-dispersive analysis; analyst A.V. Sibtsov, Institute of the Geology of Ore Deposits, Petrography, Mineralogy, and Geochemistry, Russian Academy of Sciences) and by examining petrographic thin sections under a microscope. The results are presented in Table 3.

ANALYTICAL RESULTS

As can be seen in Table 2, our samples contain from 4.94 to 38.1% Fe and from 0.09 to 30.1% Mn, and their Mn/Fe ratio varies from 0.002 to 6.08. The lowest values of this ratio are typical of crust B4-37-2 from Charlotte Bank in the South China Sea, away from island arcs. The crust containing 38.1% Fe (likely mostly in the form of goethite and hematite, Table 3) contained traces of benthic organisms. The Mn concentration in this crust (0.09%) is close to that typical of terrigenous deposits of the near-continent type of lithogenesis (0.056%) [9], i.e., the material likely contained practically no Mn oxi-hydroxides.

The variations in the Al concentrations were also significant: from 0.51% in crust B30-29-1 from the Colville Ridge in the Karmadek island arc to 9.59% in crust B5-6-79 from Esmeralda Seamount in the Mariana island arc. Mega- and microscopic examination of the samples indicate that elevated Al concentrations are caused by the presence of volcaniclastic material of basaltic and andesitic composition. The compositions of all of the crusts are shown in the Fe–Mn–Al triangular plot of Fig. 3. The systematics of the composition of the pipes in terms of proportions of ore components (Fe and Mn) and the volcaniclastic component (Al) led us to conclude that, regardless of the geographic location of their sampling sites, the Fe–Mn deposits can be clas-

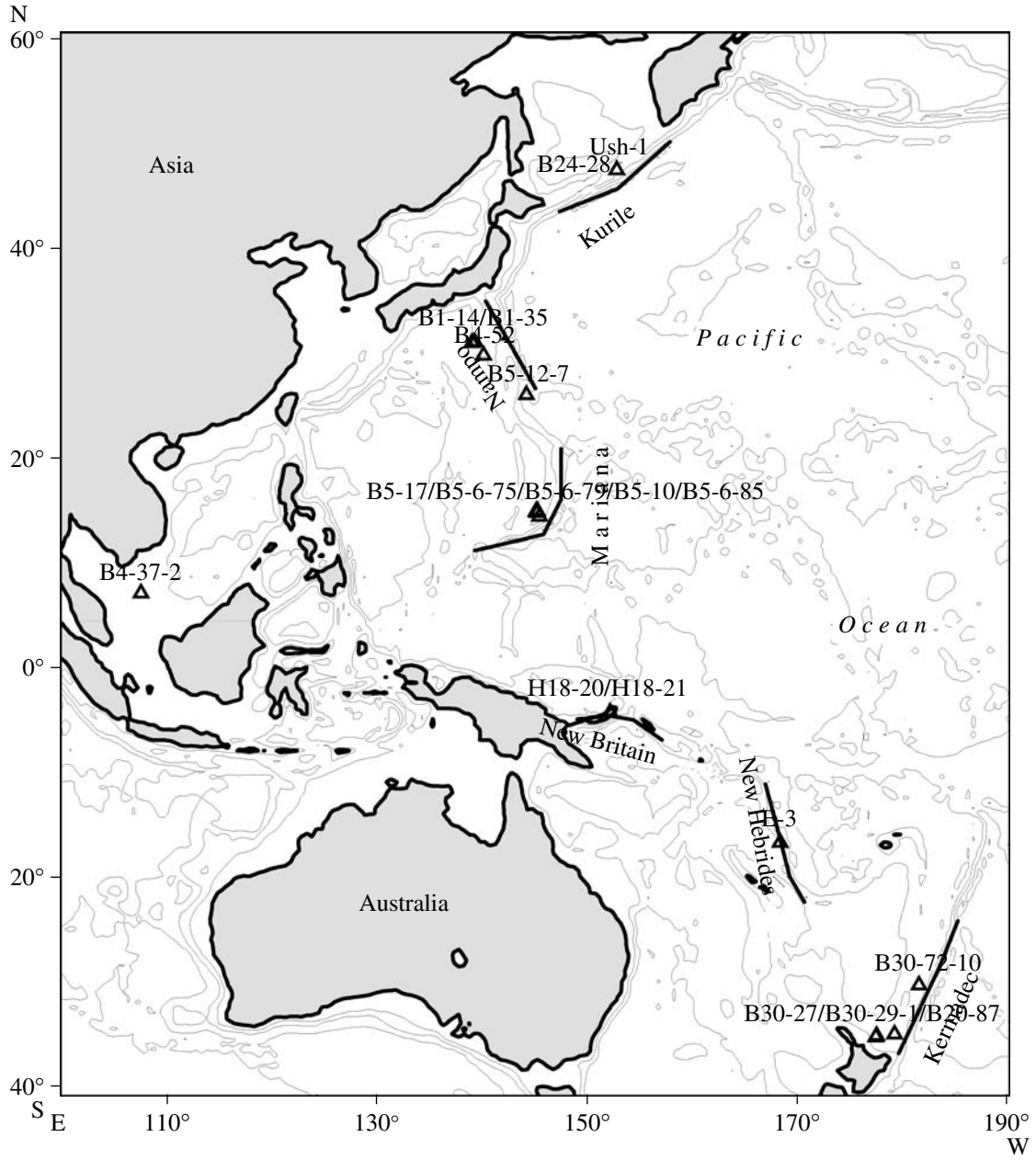

Fig. 1. Map of the West Pacific Ocean and our sampling sites of Fe–Mn depmosits in it.

sified into the following three groups: (1) with low Mn concentrations (<10% of Al + Fe + Mn), (2) with low Al contents (according to the same criterion), and (3) four samples of intermediate composition between the two above groups. It can be seen that the Fe/Al ratio in the samples of the first group is lower than in arc basalts and andesites. Fig. 3 shows the Fe/Al ratios of basalts and andesites; however, the scatter of the values in the volcanic material (basaltic, andesitic, and rhyolitic glasses, dacite lapilli, and bombs) from sediments from the Mariana island arc may be much broader: 1.1–0.27 [8].

The second group comprises samples mostly having low Al concentrations and Mn/Fe ratios close to 1, which suggests that these crusts are of hydrothermal genesis [9, 10]. However, two samples from this group (B1-14 from the Nampo island arc and H18-21/2 from Mapupi Harbor) differ from the others. Sample B1-14 is noted for a high Mn concentration (30.1%) and Mn/Fe = 6.08; and sample H18-21/2, whose composition is close to that of hydrogenic crusts, differs from these crusts in morphology: this sample represents the inner Mn-rich zone of an ore conduit. Hence, the systematics of the deposits according to their proportions of ore and nonore components did not allow us to classify them according to their morphology and genesis. The same follows from the composition of the third

Table 1. Geography and depth of sampling sites of Fe–Mn ores in the Pacific Ocean

Sample	Coordinates	Area	Region	Brief description
			Kurile island arc	
Ush-1	47° 30.6′ N, 152° 49.0′ E	0–50	Kraternaya Bay	Massive tuff-sandstone–tuff-gravelstone with dark brown Fe-rich cement
B24-28	45° 55′ N, 149° 55.5′ E	975	Shokalsky Ridge, seamount near Urup Island	Fe–Mn segregations 3 × 2 × 2 cm
			Nampo island arc	
B1-14	31° 06.7′ N, 139° 19.2′ E	1190	Smith Pinnacles	Fe–Mn crusts with a black undulating surface, lifted by a bottom-grab
B1-35	31° 01′ N, 139° 03.5′ E	960		Lavas with a Fe–Mn crust 1–5 cm thick
B1-52	29° 48.7′ N, 140° 09.2′ E	800	Sofu submarine volcanic broup	Thin platelets of volcanic glass (0.5–1 cm) cemented by Fe oxi-hydroxides
B5-12-7	26° 02′ N, 144° 13.5′ E	870	Rise between the Izu-Bonin trench and the Pacific oceanic floor	Cake-shaped Fe–Mn crust 15 cm in diameter, with a concentric structure
			Mariana island arc	
B5-6-75	14° 53.9′ N, 145° 08.6′ E	1740	Esmeralda submarine volcano	Tuff-sandstone with Fe–Mn oxi-hydroxides cement
B5-6-79	14° 55.4′ N, 145° 14.4′ E	800–850		Tuff-gravelstone with Fe–Mn oxi-hydroxides black cement
B5-6-85	14°57.2′ N, 145° 15.15′ E	250–315		Film of Fe oxi-hydroxides on fragments of volcanic rocks of yellow and red–brown color, ranging from a few fractions of a millimeter to 1.5 mm in thickness
B5-10	14° 25.5′ N, 145° 28.3′ E	1650		Fe–Mn dark brown crust on siltstone
B5-17	14° 48.0′ N, 145° 16.3′ E	1740		Dense Fe–Mn black crust, 5–15 mm thick
			South China Sea	
B4-37-2	07° 08.8′ N, 107° 34.5′ E	70	Charlotte Banck	Red-brown crusts of Fe oxi-hydroxides 3–4 m thick, with remnants of benthic organisms
			New Britain island arc	
H18-20/2	04° 14.0′ S, 152° 12.0′ E	0–50	Matupi Harbor, Rabaul caldera	Tuff-gravelstone and tuff-sandstone with a predominantly Fe-rich cement
H18-20/3b				
H18-20/3a H18-21				Pipes of intricate morphology around submarine seeps of volcanic gases and thermal waters, often filled with sedimentary material
			New Hebrides island arc	
Э-3	16° 39.5′ S, 168° 21.5′ E	430	Submarine volcano near Epi Island	Ocher-colored loose platelets, from a few millimeters to 10 mm
			Kermadec island arc	
B30-27	35° 05.7′ S, 177° 31.5′ E	1250	Southeastern slope of axial part of the Colvile Ridge	Fe–Mn crusts 2–12 mm thick on fragments of volcanic rocks
B30-29-1	35° 13.8′ S, 177° 27.8′ E	1500		Ellipsoidal Fe–Mn crust (32 × 58 mm) of loose material with a minor admixture (approximately 1%) of volcanic ash
B30-72-10	30° 16.6′ S, 178° 26.3′ W	400	Macauley submarine caldera	Fe–Mn crust up to 35 mm thick, with a black upper and dark brown lower surface
B30-87-9	34° 57.3′ S, 179° 14.3′ E	1300	Silent-1 submarine volcano	Fe–Mn crusts on fragments of volcanic rocks up to 10 mm thick

Table 2. Concentrations of chemical elements in Fe–Mn material from island arcs in the western part of the Pacific Ocean. Concentrations of Fe, Mn, Al, and P are given in %, other elements are in ppm

Element	Ush-1	B24-28	B1-14	B1-35	B1-52	B5-12-7	B5-6-75	B5-6-79	B5-6-85	B5-10	B5-17	B4-37-2
Fe	7.83	17.6	4.94	16.3	16.5	16.3	7.44	6.02	16.4	20.4	16.8	38.1
Mn	0.13	12.7	30.1	14.3	0.18	19.1	7.42	4.63	0.90	13.3	18.2	0.09
Al	8.00	2.15	2.02	2.04	6.93	1.16	7.35	9.59	7.09	1.79	0.73	3.57
P	0.23	0.48	0.19	0.52	0.17	0.66	0.08	0.05	0.11	0.53	0.58	0.30
Co	11	1374	1673	1945	23	5252	89	48	70	2065	5481	13
Cu	18	196	531	340	48	407	970	84	245	370	333	9
Ni	1	1237	2271	3191	n.d.	2417	32	46	3	1662	2917	32
Zn	56	479	690	575	70	630	102	64	93	501	475	199
Ga	15.9	10.0	15.0	8.7	15.8	9.8	20.5	18.1	17.6	8.1	7.0	12.1
Rb	9	9	21	9	5	4	12	7	12	7	4	86
Sr	363	1156	791	1126	187	1357	378	467	375	1311	1287	73
Y	18	147	49	137	30	167	23	10	21	175	190	4
Mo	17	61	445	300	66	455	33	11	15	216	378	2
Cd	0.2	2.1	12.5	4.8	0.6	5.5	0.7	3.8	0.4	3.4	3.5	0.1
Cs	0.5	0.4	3.0	0.6	n.d.	0.5	0.2	0.1	0.2	0.6	0.2	5.9
Ba	192	1426	6542	1010	90	1110	288	171	234	1179	963	165
W	n.d.	64	149	48	n.d.	86	n.d.	2	n.d.	40	69	Ì.Ó.
Tl	0.5	15.5	155	109	0.8	76.6	1.8	1.3	0.9	50.4	104	0.4
Pb	13	578	319	1731	8	1968	8	3	10	1223	1574	18
Bi	n.d.	5.4	2.6	19.4	n.d.	28.8	n.d.	n.d.	n.d.	8.8	15.6	Ì.Ó.
Th	0.61	25.7	6.34	31.0	0.37	34.3	0.78	0.46	0.80	19.0	27.9	6.02
U	1.20	11.2	3.73	13.1	2.74	18.2	1.09	0.34	0.85	12.0	15.6	2.87
La	4.5	234	54.6	198	5.1	254	6.8	3.6	6.7	249	289	8.8
Ce	10.8	744	131	839	12.7	870	14.9	7.7	15.1	492	596	16.8
Pr	1.62	60.5	10.8	39.5	1.93	54.2	2.23	1.09	2.20	54.5	57.7	1.89
Nd	7.57	254	46.9	169	10.3	227	10.6	5.0	10.1	231	242	6.5
Sm	2.15	57.7	9.79	35.3	3.23	48.3	3.22	1.53	3.11	49.6	51.2	1.2
Eu	0.87	14.2	1.57	9.31	1.10	12.5	1.07	0.60	1.06	13.0	13.7	0.21
Gd	2.71	54.9	11.3	40.3	4.11	51.2	3.73	1.74	3.63	52.7	55.7	0.81
Tb	0.43	8.23	1.69	6.11	0.69	7.81	0.66	0.29	0.57	7.91	8.27	0.12
Dy	3.00	47.0	10.2	36.4	4.58	46.9	3.98	1.80	3.76	48.6	51.1	0.70
Ho	0.67	8.20	2.01	7.13	0.97	8.77	0.82	0.35	0.75	8.77	9.64	0.11
Er	1.94	23.7	6.24	21.7	3.28	26.0	2.73	1.18	2.31	27.0	29.4	0.44
Tm	0.31	3.39	0.87	3.18	0.50	3.88	0.37	0.15	0.37	3.85	4.24	0.06
Yb	2.00	22.0	5.67	20.1	3.11	23.8	2.49	1.03	2.25	25.4	26.9	0.45
Lu	0.32	3.40	0.94	3.08	0.55	3.77	0.39	0.18	0.37	3.86	4.30	0.11
Mn/Fe	0.02	0.72	6.08	0.88	0.01	1.17	1.00	0.77	0.06	0.65	1.08	0.002

Table 2. (Contd.)

Element	H18-20/2	H18-20/3		H18-21			E-3	B30-27	B30-29-1	B30-72-10		B30-87-9
		a	b	1	2	3				1	2	
Fe	11.8	16.3	17.7	22.7	16.4	9.21	15.9	13.0	19.1	7.52	10.7	23.1
Mn	0.23	0.35	0.13	4.35	21.4	1.05	0.27	14.2	18.7	7.40	0.27	10.9
Al	6.60	5.59	6.78	4.95	1.03	6.66	5.36	2.01	0.51	7.65	8.46	1.66
P	0.21	0.72	0.13	0.15	0.15	0.21	0.29	0.32	0.59	0.05	0.12	0.56
Co	24	19	9	14	157	16	11	1264	3492	2587	97	962
Cu	40	19	24	43	39	19	35	890	346	4148	250	366
Ni	1	2	n.d.	5	97	4	3	4453	3011	490	38	1423
Zn	297	386	185	1236	2298	364	58	841	611	120	76	635
Ga	15.7	14.0	15.6	13.0	7.1	15.8	13.5	10.5	8.0	19.2	19.1	6.6
Rb	32	26	28	33	19	38	59	9	2	7	9	5
Sr	346	369	379	398	516	316	206	980	1451	291	271	1172
Y	28	28	20	24	14	38	27	48	193	25	18	153
Mo	12	11	5	7	54	7	26	190	447	292	11	220
Cd	0.2	0.4	n.d.	0.3	0.9	0.4	0.3	9.3	4.0	0.7	0.1	2.9
Cs	2.8	3.8	2.9	8.1	2.6	1.7	1.4	0.6	0.1	0.4	0.3	0.1
Ba	350	269	316	217	772	372	471	1686	1142	672	143	1170
W	n.d.	n.d.	n.d.	n.d.	n.d.	n.d.	n.d.	32	86	n.d.	n.d.	39
Tl	0.4	0.3	0.2	0.3	4.7	0.9	1.2	114	117	1.0	0.1	29.5
Pb	9	8	8	8	2	8	16	358	1838	3	3	971
Bi	n.d.	n.d.	n.d.	n.d.	n.d.	n.d.	0.1	2.2	18.4	n.d.	n.d.	6.8
Th	1.19	0.84	1.09	0.77	0.20	1.49	3.08	2.03	15.7	0.39	0.49	9.58
U	3.25	3.07	1.43	3.45	9.86	3.16	2.90	5.69	15.0	1.50	1.35	11.0
La	8.9	8.2	9.4	7.2	2.0	11.3	14.6	26.0	265	3.9	3.9	166
Ce	21.2	21.1	23.6	17.5	5.0	26.9	35.8	102	465	7.7	9.2	349
Pr	3.03	3.19	3.45	2.49	0.83	4.03	4.93	4.37	47.0	1.28	1.42	29.7
Nd	15.1	16.4	16.0	11.3	4.4	19.0	20.6	18.9	199	6.6	7.3	128
Sm	4.59	4.51	3.49	2.95	1.31	5.78	4.84	3.9	38.2	2.0	2.2	25.7
Eu	1.34	1.48	1.13	0.95	0.31	1.74	0.97	0.84	10.2	0.67	0.77	7.13
Gd	5.02	5.14	3.67	3.58	1.88	6.14	4.93	5.42	44.8	2.60	2.57	31.4
Tb	0.80	0.81	0.56	0.54	0.33	1.06	0.76	0.85	6.77	0.43	0.47	4.81
Dy	5.39	5.29	3.89	3.85	2.16	7.50	4.73	6.03	43.5	3.00	2.97	32.0
Ho	1.07	1.05	0.73	0.81	0.44	1.40	0.88	1.39	8.49	0.60	0.54	6.37
Er	3.50	3.25	2.46	2.57	1.56	4.91	3.10	4.75	27.8	1.97	2.00	20.9
Tm	0.53	0.50	0.33	0.41	0.22	0.75	0.48	0.73	4.10	0.29	0.25	3.14
Yb	3.84	3.72	2.47	2.78	1.43	5.25	2.99	4.95	25.7	1.73	1.82	19.8
Lu	0.61	0.58	0.40	0.52	0.25	0.82	0.46	0.89	3.95	0.34	0.32	3.35
Mn/Fe	0.02	0.02	0.01	0.19	1.31	0.11	0.02	1.09	0.98	0.98	0.03	0.47

Note: n.d. means concentrations below the detection limit.

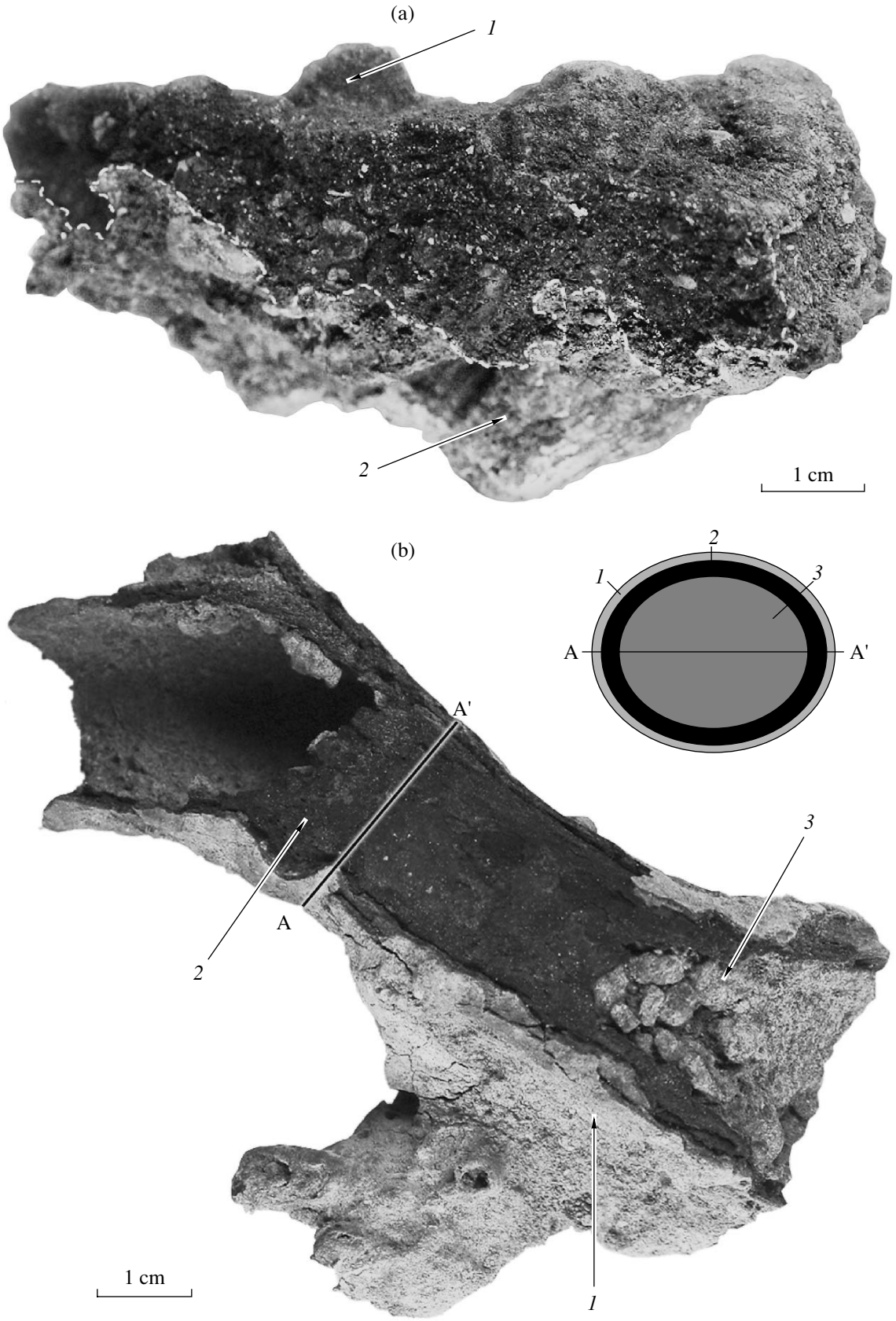

Fig. 2. (a) Fe–Mn crust (side view) of sample B30-72-10 from the Macauly submarine caldera and (b) H 18–21 pipe from the bottom of Matupi Harbor. Arrows indicate sampling sites, numerals are sample numbers.

Table 3. Mineralogy of Fe–Mn segregations from island arcs in the western part of the Pacific Ocean

Sample	Sample color	Mineralogical composition
Ush-1	Brownish black	Fe oxi-hydroxides, glass is partly palagonitized and contains quartz potassic, feldspar, and plagioclase; glass of andesite–dacite composition, phenocrysts are plagioclase, clinopyroxene, and hornblende
B24-28	Brown-black	Fe-vernadite, Mn-feroxyhyte, admixture of poorly ordered buserite-2 (poorly pronounced 10 Å reflections) and a Fe–X phase
B1-14	Brown-black	Fe-vernadite, vernadite replacing todorokite, unordered todorokite, admixtures: Mn-feroxyhyte, todorokite, and a Fe–X phase
B1-35	Black	Fe-vernadite, vernadite, semiordered asbolane-buserite
B1-52	Brown	Poorly recrystallized Fe oxi-hydroxide, sometimes in the form of globules between volcaniclastic particles of predominantly andesite–dacite composition, with plagioclase and pyroxene phenocrysts
B5-12-7	Brown-black	Vernadite, Fe-vernadite, Mn-feroxyhyte, asbolane-buserite (Ni)
B5-6-75	Black	Weakly ordered "Ca-birnessite" (basis reflections are split, additional weak network of reflections is poorly pronounced), vernadite, unordered todorokite, brown-green or brown vesicular glass (sometimes with plagioclase microlites) with phenocrysts of plagioclase, pyroxene, and olivine of basaltic composition cemented by oxi-hydroxides
B5-6-79	Black	"Ca-birnessite" (very fine-grained, unordered, in mixture with phyllosilicates), vernadite, Fe-vernadite, pale green vesicular glass with phenocrysts of plagioclase, pyroxene, and olivine of basaltic composition, occasional fragments of palagonitized glasses with Fe oxi-hydroxides
B5-6-85	Brown to foxy brown	Feroxyhyte (Fe ⩾ Mn) and protoferoxyhyte, ferrihydrite and protoferrihydrite (Mn-free), oxi-hydroxides cement brown-green glass (tuff) with phenocrysts of plagioclase, pyroxene, and olivine of basaltic composition
B5-10	Brown-black	Fe-vernadite, Mn-feroxyhyte
B5-17	Brown-black	Fe-vernadite, Fe–X phase (Si-bearing), Mn-feroxyhyte, goethite
B4-37-2	Brown	Goethite (aggregates of small acicular crystals), hematite (fine-grained)
H18-20/2	Brown	Many phyllosilicates (including nontronite), poorly crystalline Si–Fe mass, goethite, vesicular glass of andesite–dacite composition with plagioclase and pyroxene phenocrysts
H18-20/3(a)	Brown	Protoferoxyhyte (Fe⩾ Mn), basaltic glass with plagioclase, pyroxene, and olivine phenocrysts
H18-20/3(b)	Brown	Much nontronite and other phyllosilicates, poorly crystalline Si–Fe mass (sometimes Mn-bearing), goethite (aggregates of small acicular crystals)
H18-21(1)	Brown	Poorly crystalline Si–Fe mass (nontronite), ferrihydrite, occasional fragments of acid (dacite(glass, occasional fragments of plagioclase and pyroxene with rims of Fe oxi-hydroxides, Fe oxi-hydroxide composes layers of variable thickness, intercalating with nontronite around the perimeter of a pipe
H18-21(2)	Black	Unordered todorokite, asbolane-buserite, Mn oxi-hydroxides intercalating with Fe oxi-hydroxides, dendrites of Mn oxi-hydroxide in a thin calcite layer in a pipe
E-3	Brown	Poorly crystalline Si–Fe mass, goethite, acid glass (andesite-dacite), the morphology of the fragments corresponds to that of tuff, occasional phenocrysts of pyroxene and plagioclase (rare)
B30-27	Brown-black	Fe-vernadite, traces of asbolane-buserite
B30-29-1	Black	Fe-vernadite, vernadite
B30-72-10(1)	Brown-black	Fe-vernadite, vernadite, Mn oxi-hydroxides in the form of a thin film of framboidal texture, volcaniclastic material consists of porphyritic basalt (plagioclase) with a microlitic (plagioclase) groundmass, occasional fragments of plagioclase, clinopyroxene (augite), and olivine, rare fragments of palagonitized glasses with occasional segregations of Fe oxi-hydroxides
B30-72-10(2)	Pale brown	Volcaniclastic material of porphyritic (plagioclase) basalts with a microlitic (plagioclase) groundmass, single fragments of plagioclase, clinopyroxene, and olivine, occasional fragments of palagonitized glasses with rare segregations of Fe oxi-hydroxide replacing them
B30-87-9	Brownish black	Fe-vernadite, Fe–X phase, Mn- feroxyhyte, goethite, admixture of asbolane-buserite

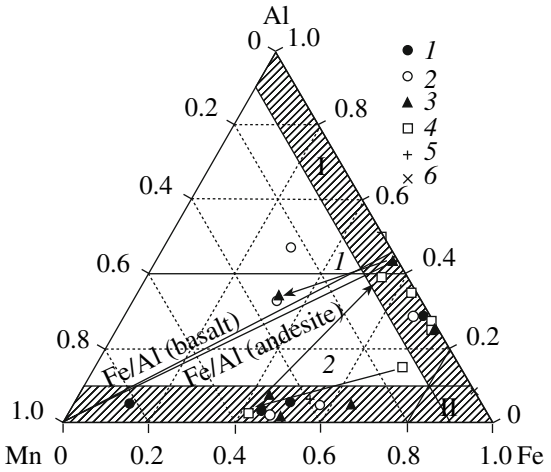

Fig. 3. Triangular Fe–Mn–Al plot for the composition of Fe–Mn mineralization from island arcs in the western part of the Pacific Ocean: (*1*) Nampo island arc; (2) Mariana island arc; (*3*) Kermadec island arc; (*4*) Matupi Harbor, New Britain Island; (*5*) Kurile island arc; (*6*) Charlotte Bank, South China Sea. Average Fe/Al ratios are also shown for arc basalts and andesites [7]. Numerals near arrows indicate changes in the composition of (*1*) Fe–Mn crust B30-72-10 (from its lower to upper part) and (*2*) feeding pipe H18-21 (from the outer zone inward).

group, which shows, along with elevated Al concentrations, high contents of Mn as well. Nevertheless, our analysis of the major-composition of the samples indicates that, if we do not consider the pipe from the Matupi Harbor (sample H18-21), the whole diversity of the deposits is characterized either by low Al concentrations at Mn/Fe ratios close to 1 or by high Al concentrations (due to the presence of aluminosilicate material) and low Mn concentrations.

An increase in the Mn concentration is associated with an increase in the concentrations of trace elements: Co, Cu, and Ni (Fig. 4). In the Mn–Fe–10(Co + Ni + Cu) diagram, our samples plot within the field of pelagic nodules and hydrogenic crusts, hydrothermal Fe–Mn deposits, and hydrothermal metalliferous sediments and diagenetic nodules from the margins of oceanic pelagic zones. The Fe-rich Mn-poor deposits are very poor in Co, Cu, and Ni. An increase in the Mn concentration in the upper part of crust B30-72-10 is also associated with fairly notable enrichment in trace elements, so that the composition of the crust shifts from the field of hydrothermal material to the field of hydrogenic material. At the same time, an increase in the Mn concentration is not necessarily associated with an increase in the concentrations of trace elements. The Mn-rich zone of pipe H18-21 and samples B5-6-79, B5-6-75, and B5-6-85 are practically not enriched in Co and Ni, and only crusts B5-6-75 and B5-6-85 show appreciable enrichment in Cu (970 and 245 ppm, respectively). Such selectivity in Cu enrichment cannot be accounted for by the adsorption of this element on Mn oxides from seawater.

Below we will discuss the variations in the mineralogy and chemistry of the Fe–Mn deposits in areas where they were sampled, going from north to south.

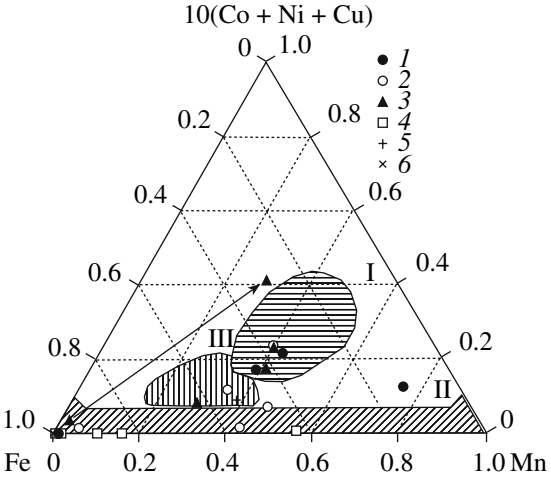

Fig. 4. Triangular Fe–Mn–10 × (Co + Ni + Cu) plot for the composition of Fe–Mn mineralization from island arcs in the western part of the Pacific Ocean: (I) pelagic nodules and hydrothermal crusts; (II) hydrothermal Fe–Mn deposits; (III) hydrothermal metalliferous sediments and diagenetic nodules of oceanic pelagic zones [11, 12]. The arrow indicates the change in the composition of Fe–Mn crust B30-72-10 form its lower surface to the upper one. See Fig. 3 for symbol explanations.

Kurile Island Arc

The deposits of the Kurile island arc were represented in our research by two samples: Ush-1 and B24-28. Sample Ush-1 was taken in Kraternaya Bay, which is an active crater of the Ushishir volcano filled with seawater. The modern subaerial and subaqual fumarole–hydrothermal activity at the bay is characterized by temperatures as high as 96°C and pH 2–3.5 [13, 14].

Both this latter fact and the topography of Kraternaya Bay are reflected in the hydrological regime of its water masses and its modern sedimentation processes. The bottom sediments of the bay have an anomalous chemical composition compared to normal (background) sediments at comparable hypsometric levels outside the bay [13, 15].

Crust Ush-1 consists of volcaniclastic material cemented with Fe oxi-hydroxides and with low concentrations of Mn, Co, Ni, Cu, Zn, Mo, Tl, Th, and some other trace elements. The P concentration was also proved to be lower than its content in sediments from the caldera (no higher than 1.85%) [13]. The REE composition is deficient in LREE with respect to clay from the Russian Platform [16], which is a typical feature of intermediate and acid volcanics (considering the low concentrations of these elements in such rocks).

Crust B24-28 has a composition opposite that of crust Ush-1. Sampled at a seamount near the island of Iturup at a depth of 975 m, it has a Mn/Fe ratio of 0.7 and contains Fe-vernadite and Mn- feroxyhyte, i.e., minerals typical of hydrothermal Fe–Mg mineralization [18]. Having low Al concentrations (2.15%), this crust is characterized by elevated concentrations of trace elements (Co, Ni, Zn, Pb, W, and Tl) and notably higher contents of Th and U. The REE composition of this material is also typical of hydrogenic crusts (Fig. 5a): the REE patterns have a positive Ce anomaly as a consequence of Ce oxidation in hydrogenic suspension in seawater [10].

Nampo Island Arc

In this publication we characterize the mineralogy and chemistry of four crusts from the Nampo island arc: samples B1-14, B1-35, B1-52, and B1-12-7. Samples B1-14 and B1-35 were collected at submarine volcanoes near the Smith Pinnacles, with B1-35 collected from the area of the 1869 submarine eruption [19–21]. The volcanoes crown the ridge that extends northeastward at an angle of 60°–70° to the trend of the Izu–Bonin island arc.

Although the sampling sites of crusts B1-14 and B1-35 are at a distance of approximately 35 km from each other, these crusts have remarkably different compositions. Crust B1-14 is much richer in Mn (more than twice as rich) but is poorer in Fe at a similar Al concentration. Both crusts are variably enriched in Co, Ni, Zn, and Mo. The W concentration in crust B1-35 is three times lower and that of Tl is almost five times lower. This crust is richer in REE and Y, and the REE composition of crust B1-35 is typical of hydrogenic material (Fig. 5b). The differences between the compositions of crusts B1-14 and B1-35 are pronounced in their mineralogy: the former contains todorokite, a mineral characteristic of hydrothermal crusts [22] (Table 2), which could result in the anomalously strong enrichment of this crust in Ba (up to 0.65%) [23].

A typically hydrogenic crust was taken at Site B5-12-7 from a wall-shaped rise that separates the Izu-Bonin trench from the Pacific Ocean. Having Mn/Fe ratios close to 1 at low Al concentrations, this crust is significantly enriched in Co (0.53%), Ni, Mo, Pb, Th, Y, and REE. The REE composition of crust B5-12-7 is practically identical to that of crust B1-35.

An example of a composition contracting those from the Nampo arc considered above is provided by crust B1-52, which was dredged from the slope of a volcano in the Sofu volcanic group 20 km west of Sofu Gan.

The Sofu submarine volcanic group belongs to the southern group of the northern segment of the Nampo island arc (Fig. 1). It composes a ridge that rises from depths of 2200–2400 m and extends nearly latitudinally, perpendicular to the Izu–Bonin island arc. The ridge has a length of 50–55 km and a width of 12–25 km [24–26] at its bottom contour and a length of 38 km at a width of 4–13 km at the isobath of 1600 m, and its slopes have angles of 9–13°. The eastern termination of the ridge is the large (17.5 × 17.5 km) Sofu volcano. Its summit rises as a pinnacle (which is likely an unweathered neck) to 99–100 m above the sea [26, 27]. A chain of volcanoes 300–700 m high occurs near the top of the ridge. Sofu Gan is a young Quaternary volcano, through which the so-called Sofu Gan tectonic line passes, separating the northern and southern parts of the Bonin island arc [26, 28–32].

Crust B1-52 has a red color due to Fe oxide-hydroxides and contains relatively abundant volcaniclastic material of andesite–dacite composition and, hence, a lot of Al (up to 7%). At the same time, it is depleted in trace elements, and its REE composition is depleted in LREE, a feature suggesting that the REE contents in this material were controlled by the content of volcaniclastic rocks (Fig. 5b). Judging from the morphology and composition, this crust is analogous to those found in Kraternaya Bay (sample Ush-1).

Mariana Island Arc

Samples B5-6-65, B5-6-79, B5-6-75, B5-17, and B5-10 were collected at various distances (of 2.2, 6.3, 13.8, 19.6, and >20 km) from the Esmeralda submarine volcano in the Mariana island arc [13].

The Esmeralda submarine volcano in the southern part of the Mariana island arc is located in its western submarine slope that faces the Philippine Sea, 28 and 35 km from the islands of Saipan and Titian, respectively. This volcano was examined more thoroughly than other submarine volcanoes of the Mariana island arc. The very first indications that Esmeralda is a submarine volcano were obtained by Japanese researchers as early as in the first half of the 20th century [33–34], and the activity of this submarine volcano was first observed in August of 1944, when sulfur dioxide bubbles rising from it were described [35]. In the second half of the 20th century, the activity of this submarine volcano was repeatedly described as causing changes in the seawater color, gas bubbles smelling of sulfur, and ash ejections [21].

Esmeralda volcano comprises three isolated submarine mounts, extending nearly meridionally, parallel to the trend of the Mariana island arc. The northern and southern mounts are extinct volcanoes partly covered with organic limestone. The central mount is the active submarine volcano of Esmeralda. This volcano rises above the crest of the Mariana island arc for ~2500 m, with its base at depths of 1500–2000 m. Its base is 15–20 km in diameter at the 1500 m isobath, and its slopes have angles of 10°–12° in the midsection of the volcanic edifice and 15°–18° near its top [13, 24, 36–40]. The top of the volcano bears a pronounced crater that opens westward. The crater is 200–300 m deep and has a

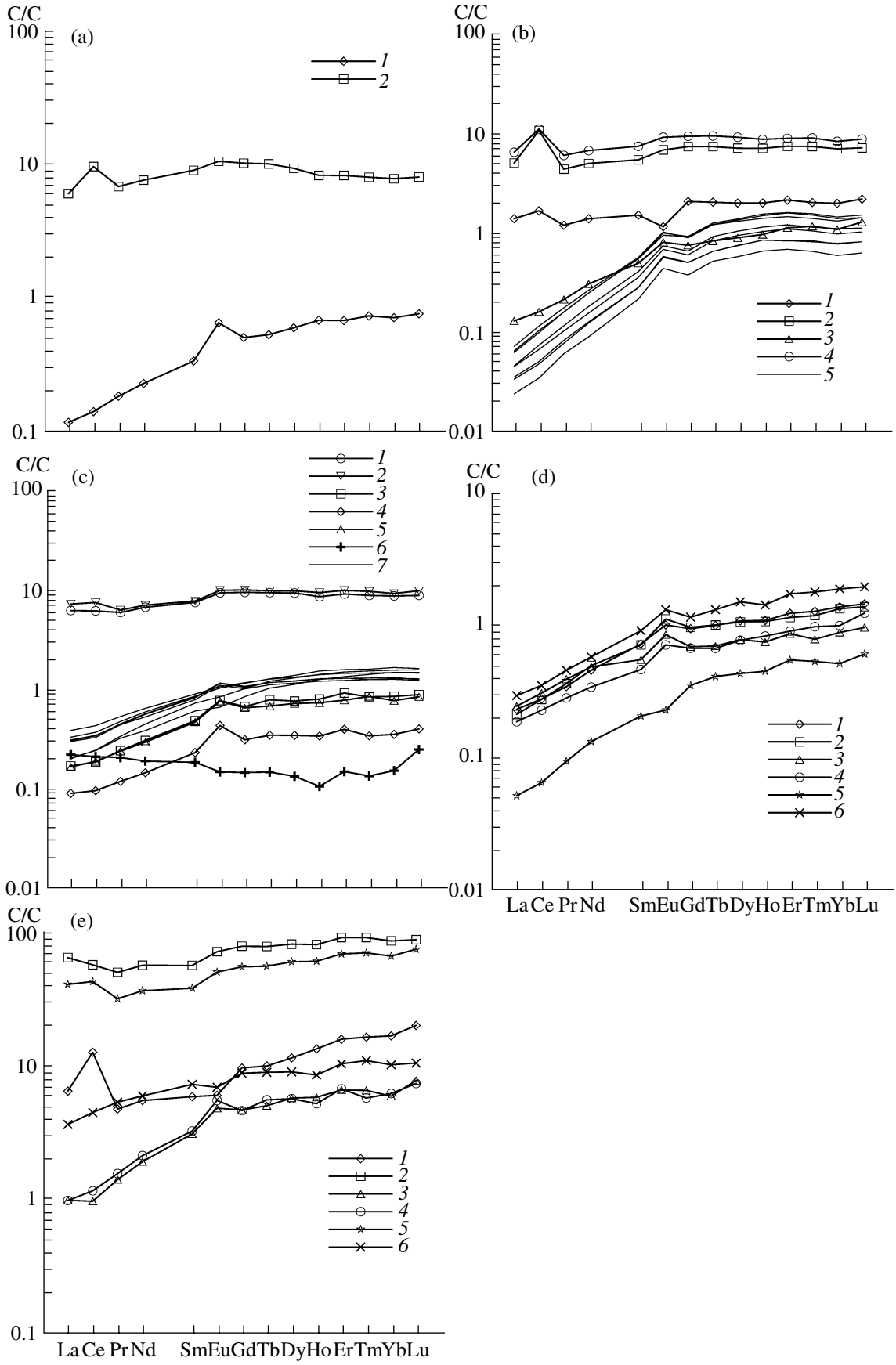
C/C
(a)
100
10
1
0.1
1
2
(b)
100
10
1
0.1
0.01
1
2
3
4
5
(c)
100
10
1
0.1
0.01
1
2
3
4
5
6
7
(d)
10
1
0.1
0.01
1
2
3
4
5
6
(e)
100
10
1
0.1
1
2
3
4
5
6
La Ce Pr Nd Sm Eu Gd Tb Dy Ho Er Tm Yb Lu

diameter of 2–3.5 km at the crest. The crater crest runs 50–100 m below the sea level. The shallowest depth of 43 m was detected at the northern crest. The northwestern crest is crowned by local peaks that rise to heights of from dozens to 100 m and are interpreted as satellite cones. Submarine fumaroles were found and examined in the northeastern slope [13, 36, 37, 39].

It was demonstrated in [13] (based on materials on 15 samples) that crusts near the volcano are richer in Fe, presumably because Fe^{2+} transported by hydrothermal solutions is less mobile than Mn^{2+}. Samples B5-6-85, B5-6-79, and B5-6-75 are quite similar in composition, and all of them contain much volcaniclastic material of basaltic composition (Table 3), which is reflected in the Al concentrations (7.1–9.6%). Volcaniclastic grains often have a vesicular texture and are coated with Fe and Mn oxides and hydroxides. The crusts are characterized by low concentrations of rare and trace elements (except Cu). The Cu concentration is not correlated with the distance from the volcano and varies from 84 to 945 ppm. Elevated Cu concentrations in the crusts near hydrothermal vents could result from the hydrothermal leaching of this element.

Crusts B5-17 and B5-10, which are located away from hydrothermal vents at the submarine volcano (at distances of approximately 20 km form it), notably differ from the crusts described above in both appearance and composition (mineralogical and chemical). They were determined to have higher concentrations of Fe and Mn, low Al contents, and very high concentrations of rare and trace elements. The Co concentrations in crusts B5-17 and B5-10 reach 0.55 and 0.21%, respectively, and are comparable with the Co concentrations in hydrogenic crusts from the western part of the Pacific Ocean [9, 41]. The REE composition of these crusts is also fairly close to those of the hydrogenic crusts [10], but both crusts have practically no positive Ce anomalies typical of hydrogenic crusts (Fig. 5c).

Charlotte Bank, South China Sea

Sample B4-37/2 was dredged from the shelf of the South China Sea in the Charlotte Bank, which has a minimum depth of 9 m [27]. Among all of our samples, this crust is likely the only one that has absolutely no relation to any volcanic source of material or hydrothermal activity. Having a relatively shallow depth (70 m) in the zone of elevated bioproductivity (remnants of benthic organisms were found at the surface), it was formed in an environment with a high content of organic matter, and this could cause high Mn mobility (in the form of oxi-hydroxides) in the sediments. The crust is colored red by goethite and hematite and contains up to 38.1% Fe, while the Al content is only 3.57%. The elevated Rb and Cs concentrations suggest the presence of significant amounts of clay minerals [42]. No other trace elements enrich the crust, and its REE composition is unusual: it is similar to that of shale over LREE and MREE (Fig. 5c), suggesting a terrigenous source of material. The elevated HREE concentrations relative to those in the shale could result from the accumulation of accessory minerals resistant to decomposition [10].

Matupi Harbor

Matupi Harbor is located in the northwestern part of the Blanche Bay in northeastern New Britain Island (Papua New Guinea, New Britain island arc) (Fig. 1). The waters of the Blanche Bay fill the Holocene Rabaul caldera, complicated by volcanic edifices of higher orders. The caldera is almost completely flooded with seawater.

Matupi Harbor is a relatively closed basin approximately 4 km^2 in area, with a maximal depth of 65 m. The harbor is open in the south and is separated from the Blanche Bay by a sandbank with depths of no more than 5–8 m in the western part and 25 m in the eastern part. In the north and east, the harbor is bounded by Rabalankaya and Tavurvur active volcanoes, to which onshore and subaquatic gas–hydrothermal vents are related. The solutions have temperatures of over 100°C, pH 3.4–3.5, and are rich in Fe, Mn, Zn, and, to a lesser degree, other trace elements [43, 44]. When mixed with alkaline seawater in the harbor, the thermal solutions are neutralized, their Fe is oxidized and then hydrolyzed, and this facilitates the enrichment (up to 30%) of particulate matter in the harbor in Fe. The maximum Mn concentration in the particulate matter reaches 1.1%, and that of Zn is 0.1% [44]. Elevated Fe, Mn, Zn, Cu, and Cd concentrations were found in sediments of the harbor, which are sands and silts with 17–35% pelite constituent [45] and remnants of shells of benthic organisms [43]. The average concentrations of Fe in the sediments of the harbor is 11.27%, and they contain (on average) 1.04% Mn, 4.06% Al, 300 ppm Zn, 53 ppm Cu, and 29 ppm Pb [45]. Sediments are oxidized at the surface and have a red color in the eastern part of the harbor but are reduced in its western part (where they have an olive-red to olive color). Fe-rich crusts and

Fig. 5. REE patterns normalized to clay form the Russian plate [16] for Fe–Mn mineralization from island arcs in the western part of the Pacific Ocean: (a) Kurile island arc: (*1*) Ush-1, (*2*) B24-28;
(b) Nampo island arc: (*1*) B1-14, (2) B1-35, (*3*) B1-52, (*4*) B5-12-7, (*5*) basalts, diabases, and altered glass form the inner slope of the Izu-Bonin trough [17];
(c) Mariana island arc: (*1*) B5-10, (*2*) B5-17, (*3*) B5-6-75, (*4*) B5-6-79, (*5*) B5-6-85, (*6*) B4-37-2, South China Sea, Charlotte Bank; (*7*) tephra layers of basalt–andesite–rhyolite glasses, dacite lapilli, and bombs form the Mariana trough [8];
(d) Matupi Harbor: (*1*) H18-20/2, (*2*) H18-20/3(a), (*3*) H18-20/3(b), (*4*) H18-21(1), (*5*) H18-20(2), (*6*) H18-21(3);
(e) Kermadec island arc: (*1*) B30-27, (*2*) B30-29-1, (*3*) B30-72-10(1), (*4*) B30-72-10(2), (*5*) B30-87-9, (*6*) E-3, New Hebrides.

pipes found and described in sediments of the harbor were thought to be fragments of conduits of mineralized solutions [13, 45].

We examined four samples (Table 1), two of which (H18-20/2 and H18-20/3b) are Fe-rich crusts and the other two are pipes, one having an equant cross section and branches (sample H18-21) (Fig. 2b) and the other (sample H18-20/3a) having a flattened shape. The walls of the pipes are zonal due to variations in their content of Fe oxi-hydroxides (in sample H18-20/3a) or, firstly, Fe oxi-hydroxides and then Mn oxi-hydroxides (sample H18-21). The inner Mn-rich zone is overlain in places by a calcite zone of variable thickness with occasional MnO_2 dendrites. We managed to sample two zones of distinct color from the pipe of sample H18-21; the third sample represented the loose material that fills the inner space of the pipe. The latter is likely the sedimentary material of the harbor that filled the pipe after the cessation of hydrothermal circulation through it. The chemical composition of sample H18-21/3 is also close to the composition of sedimentary material of the harbor (see [43, 45]). The Fe-rich crusts of sample H18-20/2 and H18-20/3b and sample H18-20/3a (the wall fragment of a pipe) have a similar composition. All of these samples contain relatively a lot of Al (5.6–6.8%), thus confirming the presence of volcanic–terrigenous material in them. The Fe concentrations of the crusts are higher than those of the sediments, because Fe oxi-hydroxides are contained in the cement, but the Mn concentrations are lower than in the sediment (0.13–0.35%) and close to those in terrigenous sediments in the marginal parts of oceans [6]. The Zn, Cu, and Pb concentrations are close to those published in [43, 45], and all of these values (except Zn) are much lower than those of the hydrothermal crusts [9].

The Fe- and Mn-rich zones of the pipe of sample H18-21 (Fig. 2b) seem to be the most interesting. The outer zone contains more Fe than in our other samples from the harbor, more Mn, less Al, and almost four times more Zn (1236 as compared to 185–386 ppm). No significant concentrations of any other elements were detected. The inner Mn-rich zone is noted for, first of all, higher concentrations of Mn (by a factor of 4.9) and Zn (by a factor of 1.9) at a low Al concentration (1.03%). Compared to the outer Fe-rich zone, the Mn-rich zone is most strongly enriched in Ni (its concentration is 20 times higher), Tl (13.5 times higher), Co (11 time higher), Mo (7.2 times higher), Ba (3.6 times higher), U (2.9 times higher), and Cd (2.8 times higher) (Table 4). Judging by descriptions, a similar Fe–Mn pipe was examined and documented in [45]. Its only significant difference from our pipe is that the Mn-rich zone in the latter occupied an outer position relative to the Fe-rich zone, and the Mn concentration gradually decreased inward. Nevertheless, the Mn-rich zone was also enriched in Zn (by a factor of 7.1), Pb (2.1), and Cu (2.5), with none of them noted in sample H18-21/2 (Table 2).

The Th, Y, and REE concentrations in sample H18-21 are at a minimum in the zone enriched in Mn. The REE composition of this zone notably differs from those of all other samples of Fe-rich material from Matupi Harbor in that it has an Eu anomaly. The other samples show a deficit of LREE relative to HREE and seem to inherit their REE composition from the aluminosilicate material (Fig. 5d).

New Hebrides Island Arc

Our Fe-rich crust sample (sample E-3) was dredged from an active submarine volcano in the northern wall of the Epi caldera (volcanoes Epi A, Epi B, and Epi C) northeast of the southeastern margin of Epi Island in the New Hebrides island arc. The area is characterized by very high volcanic activity: submarine eruptions and gas–hydrothermal activity related to Karua volcano (which is located 10–12 km southeast of the Epi caldera and Epi A, Epi B, and Epi C submarine volcanoes) were repeatedly registered there in the past. Simultaneous eruptive activity was observed in this area in February 1953 at the three submarine volcanoes of the Epi caldera. New islands were almost always formed after the eruptions of these volcanoes and then demolished by marine abrasion. When samples were collected during Cruise 18 of the R/V *Akademik Nesmeyanov*, activity was observed at one of the submarine volcanoes (Epi B) of the caldera. Marine geological studies indicate that Karua volcano is made up of basalts, and the predominant material of the submarine slopes of Epi volcano is poorly sorted deposits with Fe-rich crusts.

One such fragment (sample E-3) is poor in Mn but rich in Fe and Al, a fact indicating (along with the mineralogy of this sample, Table 3) that the crust consist of volcanic material (the shapes of the fragments resemble those in tuff) cemented by Fe oxi-hydroxides. The crust is characterized by low concentrations of trace elements and its REE composition is deficient in LREE and Eu. The negative Eu anomaly may be accounted for by admixtures of volcanic rocks of acid or intermediate composition (Fig. 5e).

Kermadec Island Arc

Four samples of Fe–Mn crusts (B30-27, B30-29-1, B30-72-10, and B30-87-9) were dredged from the Kermadec island arc (Table 1). The crusts were taken from the vicinity of modern submarine volcanoes whose activity is associated with the discharge of hydrothermal solutions and the deposition of hydrothermal sulfide ores [47, 48]. Samples B30-27 and B30-29-1 were dredged at the southeastern slope, near the axial part of the Colville Ridge, which is a remnant (degrading) island arc. Sample B-30-87-9 was lifted from the slope of the Silent-1 submarine volcano in the southwestern segment of the Kermadec island arc [49].

Judging from their chemical composition and mineralogy, crusts B30-27, B30-29-1, and B30-87-9 are

hydrogenic. They contain 2% Al and have Mn/Fe = 0.5–1 and elevated concentrations of Co, Cu, Zn, Mo, W, Tl, and Pb. Crust B30-27 is additionally weakly enriched in hydrolysate elements (REE, Y, and Th) from seawater. The REE compositions are characterized by a deficit in LREE, as is typical of volcaniclastic material of basic and intermediate composition, and selective enrichment in Ce (a feature that is typical of hydrogenic oxi-hydroxides) (Fig. 5e). Crusts B30-29-1 and B30-87-9 have very high REE concentrations compared to those in hydrogenic crusts from the Pacific Ocean [10], but they show almost no positive Ce anomalies (1–1.2).

It is pertinent to separately discuss the composition of crust B30-72-10. This sample was lifted in the area of the Macauley submarine caldera [50], not far from Macauley Island. As can be seen in Fig. 2a, the crust is zonal, with its lower and upper parts significantly different from each other. In contrast to other crusts from the Kermadec Ridge, crust B30-72-10 consists of volcano-terrigenous material cemented by oxi-hydroxides. The cement in the lower and upper parts consists of Fe oxi-hydroxides. The enrichment of this material in Mn (by a factor of 27 in the upper part of the crust relative to its lower part) was associated with enrichment in trace elements: Co (by a factor of 27) > Mo (26) > Cu (17) > Ni (13) > Tl (7) > Ba (4.7) > Zn (1.6) (Table 4). The concentrations of Pb and hydrolysate elements did not change, and the REE composition of the material is characterized by a deficit in LREE and was likely inherited form volcaniclastic material (Fig. 5e).

DISCUSSION

The Fe–Mn deposits from island arcs in the West Pacific Ocean discussed in this paper remarkably differ in both chemistry and mineralogy. These differences were controlled by variations in the contributions of the probable material sources: volcanic (due to the halmyrolysis of volcanic rocks), hydrothermal, and hydrogenic. The composition of the Fe–Mn deposits may have been controlled by a single or several sources. Our task was to use the chemical and mineralogical composition of these deposits, their morphology, and distance from hydrothermal sources in order to identify one or more predominant sources of material for individual crusts and their groups.

The volcanic source of material is usually understood as loose volcanic material that underwent multiple redeposition and mechanical reworking [51]. Volcaniclastic material contained in bottom deposits can be produced by the eruption and subsequent transport of solid material with water and air currents and by the weathering of magmatic rocks. The contribution of a volcanic–terrigenous source can be evaluated from the Al content of the deposits, an element contained in volcanic rocks mostly in the form of aluminosilicates. The Al concentration in volcanic rocks at island arcs, mostly andesites and basalts, may vary within fairly broad limits: from 6 to 11% [7]. Tephra in the Mariana island arc contains 6.26–8.26% Al [8], and the rocks and glasses dredged from the Izu–Bonin trench contain 7.23–8.58% Al [17]. Our samples have Al/(Al + Fe + Mn) > 10% and contain 4.95–9.59% Al, much of it in aluminosilicates (Table 3, Fig. 3). At such Al concentrations in the bottom deposits, its supply from other sources can be neglected. According to data in [52], the fraction of Al not bound to Fe and Mn oxi-hydroxides depends on the content of the lithogenic component in the crusts and decreases as the total Al concentration decreases (within the range of 0.2–2.6%). The fraction of reactive (related to pelites) Al (determined by leaching with 1 M $NH_2OH \times HCl$ + 25% CH_3COOH [53]) in a hydrogenic crust on sediments in the South Pacific Ocean was 29% at a total Al content of 4.52% [54].

Volcano-terrigenous material in Fe–Mn deposits predetermines some parameters of their trace-element composition. If all of our samples are grouped according to their Al contents (9.59–4.95% and <2.15%) and their average compositions (Tables 4, 5) are considered, it can be seen that samples with high Al contents are depleted in trace elements (except Tl, Cs, and Rb). The behavior of Ga closely resembles that of Al because of the similar chemical properties of these elements [55]. A distinctive feature of the samples with high Al concentrations is the inheritance of their REE composition from the volcano-terrigenous material, with a pronounced deficit in LREE and a low positive Eu anomaly (Fig. 6). It is thus reasonable to suggest that the samples with high Al contents were formed at a high enough rate at a negligible contribution of hydrogenic material, whose accumulation rate is much lower.

In averaging the compositions of samples with high Al concentrations (Tables 4 and 5), we did not take into account data on the upper surface of crust B30-72-10 and Fe-rich crust B4-37-2. Crust B-4-27-2 has a low Al concentration of (3.57%) and a high Fe content (38.1%). This crust is depleted in trace elements, which makes it similar to other Fe–Mn deposits with volcano-terrigenous material. However, the REE composition of this crust testifies that the source of its material was probably terrigenous (Fig. 5c) and close in composition to shale or clay [10]. The low REE concentrations suggest that the content of clay material was not high, which also follows from the elevated Rb and Cs concentrations relative to those in the volcano-terrigenous source.

The upper surface of crust B30-72-10 is notably enriched in Co, Cu, Ni, Zn, Mo, and Ba, i.e., elements usually related to Mn oxi-hydroxides in hydrogenic materials (Tables 4, 5) [9, 10, 52, 54]. At the same time, the concentrations of REE, Y, Pb, and Th in the upper and lower surfaces of the crust remain low and practically unchanging, and the REE composition is controlled by that of the volcanics (Fig. 5e).

The composition of the hydrogenic source is controlled by particulate Fe and Mn oxi-hydroxides, which

Table 4. Average concentrations and enrichment coefficients of Fe–Mn deposits in island arcs in the western part of the Pacific Ocean

Element	C1	C2	C3	C1/C2	C3/C2	C4/C5	C6/C7
Fe	18.5	13.6	1.22	1.4	0.1	0.7	0.7
Mn	15.3	1.72	41.9	8.9	24	27	4.9
Al	1.43	6.97	0.16	0.21	0.02	0.90	0.21
P	0.56	0.21	0.08	2.71	0.4	0.43	0.98
Co	2939	38	32	78	0.8	27	11
Cu	337	161	338	2.1	2.1	17	0.9
Ni	2265	15	338	156	23	13	20
Zn	558	238	628	2.3	2.6	1.6	1.9
Ga	8.3	16.2	19.1	0.5	1.2	1.0	0.5
Rb	6	21	9.35	0.3	0.4	0.8	0.6
Sr	1265	340	611	3.7	1.8	1.1	1.3
Y	166	22	0.77	7.4	0.03	1.4	0.6
Mo	297	20	1481	15	76	26	7
Cd	3.7	0.7	13.9	5.4	19.9	12	2.8
Cs	0.4	2.0	0.077	0.2	0.04	1.5	0.3
Ba	1143	249	2084	4.6	8.4	4.7	3.6
W	62	2	0.95	34	0.5	–	–
Tl	71.6	0.7	16.7	102	24	7	14
Pb	1412	8	7	167	0.8	1	0.2
Bi	15	0.1	0.2	166	1.7	–	–
Th	23.3	0.95	0.39	24.5	0.4	0.8	0.3
U	13.7	1.97	0.99	7.0	0.5	1.1	2.9

Note: C1—average concentrations of elements in hydrogenic crusts: B24-28, B1-35, B5-10, B5-12-7, B5-17, B30-29-1, and B30-87-9; C2—average concentrations of elements in Fe–Mn deposits with >4.95% Al, except samples H18-21(3), H18-21(2), and B30-72-10; C3—average for two crusts from the Fiji Basin [46]; C4—sample B30-72-10(1); C5—sample B30-72-10(2); C6—sample H18-21(2); C7—sample H18-21(1).

are formed in close association. This association is already formed in the upper part of the water column. Oxi-hydroxides adsorb trace elements from seawater. The irreversible character of sorption processes is pronounced more strongly for Co, Ce, and Tl with a change in their oxidation state: $Co^{2+} \longrightarrow Co^{3+}$, $Ce^{3+} \longrightarrow Ce^{4+}$, and $Tl^{1+} \longrightarrow Tl^{3+}$. The oxidation reaction of Ce, Tl, and Co proceed in the upper part of the water column on particulate matter, where Mn oxidizes [10, 56–58]. Low-mobile species of these elements enrich hydrogenic crusts. Even if the amount of the diagenetically reduced and then re-oxidized material is taken into account, the material of these crusts seems to most closely approximate the composition of the oxi-hydroxide suspension, because it is practically independent of the composition of the source [41]. High Co, Ce, and Tl concentration are typical only of hydrogenic oxi-hydroxide material, explicitly indicating that the crusts were formed in relation to relatively slow sorption and oxidation processes. High Co concentration in hydrogenic crusts is a specific (and the most remarkable) feature of hydrogenic material [3, 9–11, 41, 52]. Practically all of our samples of Fe–Mn crusts contained less than 2.15% Al and >962 ppm Co, excluding only two instances: the upper zone of crust B30-72-10 (2587 ppm Co at 7.65% Al; this material was discussed above) and Mn zones in feeding pipes found in Matupi Harbor [sample H18-21(2)]. The latter sample contained 1.03% Al and only 157 ppm Co. Sample H18-21(2) significantly differs from the hydrogenic crusts in both mineralogy (the sample contains todorokite, while the crusts contain Fe-vernatite, vernadite, and feroxyhyte) and morphology (this sample represents the inner zone of a feeding pipe) (Fig. 2b, Table 3).

The hydrogenic crusts contain Co in vernadite mostly in the oxidation state of +3 [59]. The close association of Co and Mn is confirmed by the results of leaching the hydrogenic crusts. The dissolution of Mn oxi-hydroxide results in an almost 100% yield of Co leachate into the solution [46, 52, 54]. It was demonstrated for a great number of hydrogenic hydrothermal crusts from the Pacific Ocean that their enrichment in Co depends on the growth rate of the crusts [3, 60]: the higher the Co content, the lower the growth rate of the

Table 5. Average REE concentrations and their enrichment coefficients

Element	C1	C2	C1/C2	C4/C5	C6/C7	Fe–Mn crusts from the Pacific Ocean	Basalt–andesite glasses from the Mariana Trough	Clay from the Russian Platform
La	236	7.2	33.0	1.00	0.28	243	12.23	37.5
Ce	622	17.2	36.1	0.84	0.28	1041	27.01	74.8
Pr	49.0	2.51	19.5	0.90	0.33	44.0	4.08	8.6
Nd	207	11.84	17.5	0.90	0.39	202	19.04	32.2
Sm	43.7	3.25	13.4	0.95	0.44	40.0	5.41	6.2
Eu	11.4	1.03	11.1	0.87	0.32	10.0	1.58	1.3
Gd	47.3	3.71	12.7	1.01	0.52	48.0	5.82	5.21
Tb	7.13	0.60	11.9	0.90	0.61	8.0	0.97	0.79
Dy	43.6	3.93	11.1	1.01	0.56	42.0	6.24	4.88
Ho	8.20	0.79	10.4	1.12	0.54	8.0	1.28	0.96
Er	25.2	2.58	9.8	0.98	0.61	25.0	3.78	2.78
Tm	3.68	0.38	9.6	1.14	0.55	3.0	0.56	0.41
Yb	23.4	2.59	9.0	0.96	0.52	23.0	3.76	2.73
Lu	3.67	0.43	8.6	1.05	0.49	3.8	0.55	0.41

Note: C1—average concentrations of elements in hydrogenic crusts: B24-28, B1-35, B5-10, B5-12-7, B5-17, B30-29-1, and B30-87-9; C2—average concentrations of elements in Fe–Mn deposits with >4.95% Al, except samples H18-21(3), H18-21(2), and B30-72-10; C4—sample B30-72-10(1); C5—sample B30-72-10(2); C6—sample H18-21(2); C7—sample H18-21(1).
Data are reported on the average composition of hydrogenic Fe–Mn crusts from the Pacific Ocean [10], basalt–andesite glasses in tephra from the Mariana Trough [8], and clays from the Russian Platform [16].

crust. Hence, the identification of a hydrogenic source of material in the crusts based on elevated Co, Cu, and Ni concentrations (Fig. 4) seems to present a reliable enough criterion, although it is not always corroborated by data on other elements.

The predominant ore minerals of the crusts are Fe and Mn oxi-hydroxides. Along with these minerals, the crusts can contain lithogenic (for example, volcano-terrigenous) material (aluminosilicates and various authigenic minerals, such as carbonates, apatite, barite, and zeolites). In the presence of a significant amount of volcano-terrigenous material, Fe (but not Mn) is contained in the crusts not only in the form of oxi-hydroxides but also (in a significant amount) as aluminosilicates, depending on the composition of the volcanic rocks. Judging from the average composition of island arcs [7], the Fe concentration varies from 2.35 to 8%, while the Mn concentrations vary from 0.06 to 0.14%. Thus, the content of volcano-terrigenous material almost has no effect on the Mn content in the Fe–Mn deposits, therefore, all Mn is contained in them as oxi-hydroxides.

Considering Co accumulation relative to Mn, which is assumed as an indicator of the oxi-hydroxide component of the material, it can be seen that the Co content exponentially increases as the Mn concentration increases (Fig. 7a). Two samples [B1-14 and H18-21(2)] are enriched in Mn relative to the main group of samples, and one of them [sample B30-72-10(1)] is enriched in Co. Sample H18-21(2) represents a Mn-rich zone in a feeding pipe. The source of Co for it could be mixed seawater and hydrothermal solutions. Another redox-sensitive element closely related to Mn is Tl (Fig. 7b). It shows a distribution relative to Mn close to that of Co, although two of our samples show anomalous distributions [samples B1-14 and H18-21(2)]. The Ce and Pb distributions copy that of Tl relative to Mn (Fig. 7d). A certain Mn excess was detected in the same samples in which U and Mo occur in excess (Figs. 7c, 7e). The Ba distribution relative to Mn is the only one without any exceptions (Fig. 7f). Data on the comparison of the behavior of elements in the Fe–Mn deposits relative to major components of the oxi-hydroxide constituent lead to the conclusion that an increase in the content of the oxi-hydroxide component results in an increase in the concentrations of trace elements.

According to some of their mineralogical and compositional features, seven crusts (B24-28, B1-35, B5-10, B5-12-7, B5-17, B30-29-1, and B30-87-9) can be regarded as predominantly hydrogenic. These features are as follows: low Al concentrations and, consequently, a low content of volcano-terrigenous or any other lithogenic material; an Mn/Fe ratio close to 1; high concentrations of elements with varying oxidation states when adsorbed on Mn-bearing particulate matter suspended in water (these elements are Co, Tl, and Ce); high REE concentrations and REE composition close to the average REE composition of hyrdogenic crusts in the Pacific Ocean (Fig. 6); and the predominant Mn

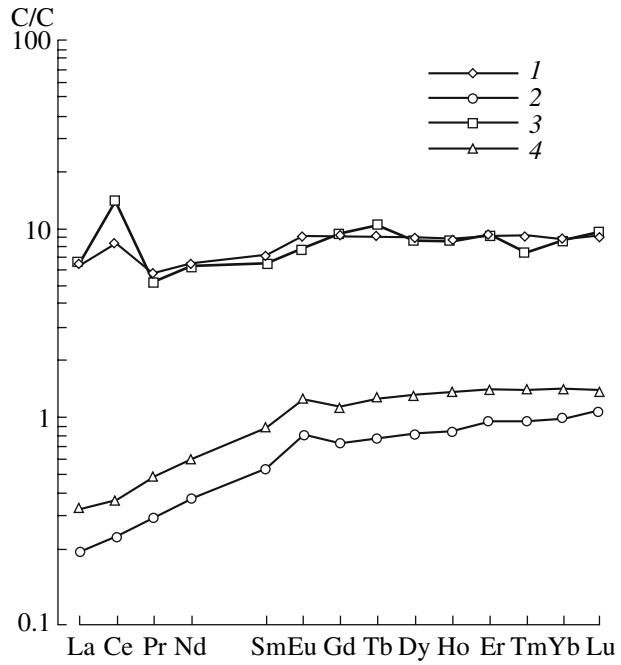

Fig. 6. (*1*) Average REE composition of hydrogenic Fe–Mn crusts from island arcs (C1) (Table 5); (*2*) Fe–Mn deposits with >4.95% Al from island arcs (C2); (*3*) hydrogenic Fe–Mn crusts from the Pacific Ocean [10]; (*4*) basalt–andesite glass in tephra form the Mariana trough [8]. All patterns are normalized to clay from the Russia plate [16].

minerals: Fe-vernadite, vernadite, and feroxyhyte (Table 3). The average composition of hydrogenic crusts studied in the course of our research is presented in Tables 4 and 5 (samples of group C1). The average Y/Ho ratio for seven samples is 20.3 (Fig. 8) and falls, according to [61], within the range of 17–25 typical of hydrogenic crusts.

Group C2 of the samples (Tables 4, 5) comprises materials with >4.95% Al containing volcano-terrigenous material, sometimes with traces of halmyrolysis of volcaniclastic particles (palagonization of glass with the development of aggregates of Fe oxi-hydroxides, which were identified in thin sections under a microscope), and cement of Fe (and, to a lesser degree, Mn) oxi-hydroxides. This group of samples has low concentrations of trace elements, REE compositions similar to those of volcanic rocks (Fig. 6), and Y/Ho = 28.4, which corresponds to this ratio of island-arc basalts (27.7±2.7) [61]. According to its Y concentration, this group of samples also notably differs from hydrogenic crusts (Fig. 8).

In Fig. 8, the group with low Y and Ho concentrations includes all of our samples. It also includes two samples with low Al concentrations (2.01–2.02%; samples B1-14 and B30-27) which were taken at the Nampo and Kermadec island arcs, respectively (Table 1, Fig. 1). These samples have unusual REE compositions (Figs. 5b, 5e), which is noted for the presence of Ce anomalies (which are typical of hydrogenic crusts) at generally relatively low REE concentrations. At the same time, their REE composition is characterized by an Eu deficit, a feature that still has not found an adequate explanation. The crusts are variably enriched in Mn (Mn/Fe = 6.08 and 1.09) and bear trace-element concentrations (including those of hydrolysate elements, such as REE, Y, and Th) comparable to those in hydrogenic crusts. The contents of Ba, Cd, W, and Tl are at a maximum in crust B1-14, compared to those in other our samples (Fig. 7). Crust B30-27 bears the highest concentrations of Ni (4453 ppm) and Zn (if discrete zones of pipe H18-21 are not included in consideration) at elevated Ba and Cd contents. Crust B1-14 contains todorokite, vernadite replacing todorokite, and Fe-vernadite (Table 3). The presence of todorokite testifies to the hydrothermal genesis of this crust [22]. Similar crusts are widespread in the western part of the Pacific Ocean, and data on their composition are summarized in [62]. The common compositional features of these crusts are as follows: their Mn oxi-hydroxides are todorokite, the Mn concentration is usually >40%, and the crusts contain elevated concentrations of Ba, Mo, and, occasionally, Ni. The average composition of two crusts that have high Mn concentrations and were collected in the North Fiji Basin is presented in Table 4 (C3). In order to consider the enrichment of this type of crusts in trace elements, their concentrations of trace elements (C3) were normalized to those in crusts with high Al concentrations (C2).The reason for this normalization is the idea that the cementing of the volcaniclastic material with Fe and Mn hydrothermal oxi-hydroxides is the first step to developing mineralized hydrothermal crusts. The conclusion about the hydrothermal source of the Fe and Mn oxi-hydroxides in deposits with high Al concentrations seems to be sound enough and follows from the nearby plotting of most of our samples to the hydrothermal fields that can be sources of oxi-hydroxide species of Mn and, sometimes, of Fe (because of the halmyrolysis processes). This conclusion is also corroborated by the mineralogy of the Mn oxi-hydroxides, which consist of todorokite and "Ca-birnessite" and have low concentrations of Co and other trace elements. The evolution of these deposits (C2) could proceed in two ways: via an increase in the supply of material from the hydrothermal source alone and via the accumulation of Mn oxi-hydroxide (C3) or a decrease in the supply of hydrothermal material and, consequently, an increase in the content of hydrogenic material with characteristics close to those of C1.

Our samples do not include any Mn crusts with >40% Mn. According to literature data [46, 62], the enrichment of hydrothermal crusts in Mn is associated with an increase in the concentrations of, first of all, Ni, Mo, Cd, Ba, and Tl (Table 4, column C3/C2). Our crusts B1-14 and B30-27 are also enriched in these elements (Fig. 7). While crust B30-27 is distinguished only by its Ni concentration, which is the highest among our samples, crust B1-14 contains 30.1% Mn at maximum concentrations of Ba, Cd, Tl, and W and an

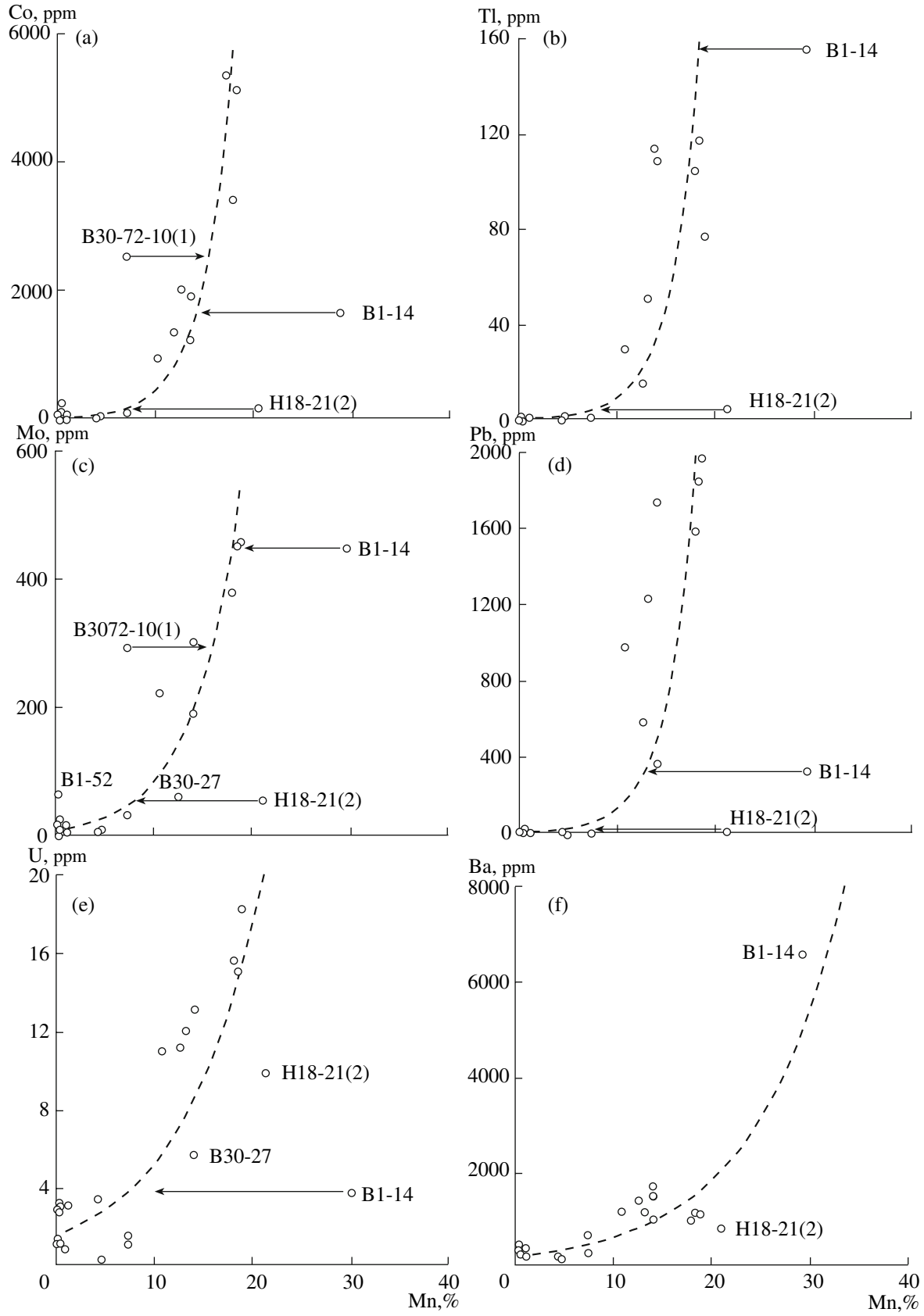

Fig. 7. Changes in the concentrations of trace elements relative to the Mn concentrations in Fe–Mn mineralization from island arcs in the western part of the Pacific Ocean. Dashed lines show exponential functions fitting the data, except for samples whose numbers are shown in the plots. Arrows indicate the change in the location of the data points with changing Mn concentration.

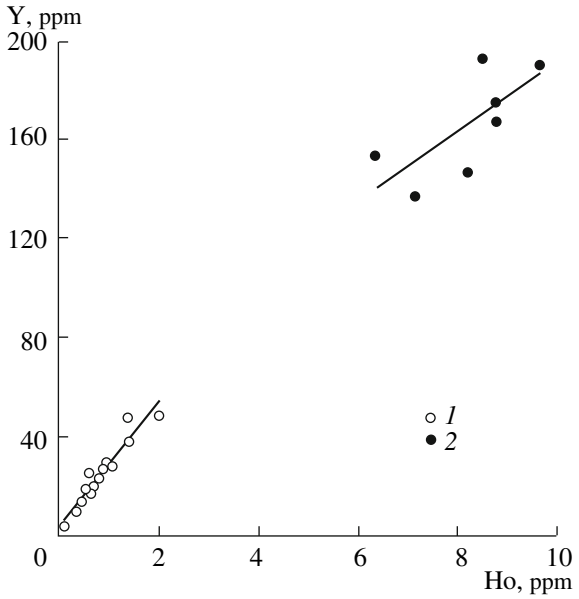

Fig. 8. Correlation between the Y and Ho concentrations in samples of Fe–Mn deposits from island arcs in the western part of the Pacific Ocean: (*1*) all samples except for hydrogenic crusts; (*2*) hydrogenic crusts.

almost maximum Mo concentration. All of these chemical features, as well as the presence of todorokite, of crust B1-14 make it (and, to some extent, crust B30-27 as well) similar to the hydrothermal mineralization described in [46, 62]. Phase analysis of the crusts from the North Fiji Basin indicates that Ba, Cd, Tl, and W for the most part enrich the Mn oxi-hydroxides in them [46, 62]. However, along with obvious traces of a hydrothermal source of material, these crusts display discernible indications of the influence of a hydrogenic source. The latter affects the mineralogy of crust B1-14, which contains Fe-vernadite and Mn-feroxyhyte, minerals typical of hydrogenic crusts [9, 22, 63]. The supply of hydrogenic material seems to result in a drastic increase in Co concentration in crusts B1-14 and B30-27, along with an increase in the concentrations of Y, Th, and REE, i.e., hydrolysate elements related to Fe oxi-hydroxides of hydrogenic genesis. The REE complex of this material shows positive Ce anomalies, which are typical of hydrogenic crusts [10].

The initial development of Mn crusts is vividly illustrated by sample B30-72-10 (Tables 4, 5). The upper surface of the volcaniclastic material originally cemented by Fe oxi-hydroxides is overlain by thin layers of Mn oxi-hydroxide (Table 3), which imparts a black–brown color to the originally pale brown material. Mn addition was associated with the enrichment of the crust in trace elements, with this crust most significantly enriched in the same elements as in crusts B1-14 and B30-27 (see above and compare columns C4/C5 and C3/C2 in Table 4). The only exceptions are Co and Cu. As was shown for hydrothermal crusts B5-6-75 and B5-6-85 from the Esmeralda submarine volcano, Cu can also become enriched in the crusts by hydrothermal processes, whereas Co enrichment is known to occur only in the water mass on particulate Mn oxi-hydroxides, with the degree of this enrichment depending on the growth rate of the crust [3]. The hydrogenic nature of Mn oxi-hydroxide in the crust follows from the occurrence of Fe-vernadite and vernadite, typical oxi-hydroxide Mn minerals in hydrogenic crusts (Table 3). One of the significant differences of the upper part of the crust from hydrogenic materials is the virtual absence of hydrogenic Fe oxi-hydroxides. Their presence can be evaluated using trace elements related to Fe oxi-hydroxides in hydrogenic crusts: REE, Y, Th, and, to some extent, Pb [9, 10, 46, 52, and others]. As can be seen from Tables 4 and 5, Mn accumulation in the upper part of the crust was not associated with its enrichment in Fe and related elements. This conclusion also follows from the REE composition of this material, with this composition remaining practically identical in both parts of the crust and inheriting that of the basalts, except only for the very weakly pronounced negative Ce anomaly in the upper part of the crust (Table 3, Fig. 5e). Mn and Fe can be supplied separately only in the hydrothermal process or during diagenetic transformations. In any event, Co is not significantly enriched, and the mineralogy of the Mn oxi-hydroxides is more consistent with the hydrogenic nature of the material. The only fact in conflict with this conclusion is the presence of Fe oxi-hydroxide. It can only be hypothesized that the selective Co enrichment was possible thanks to its high concentrations in the seawater, which could be supplied by hydrothermal solutions from the Macauly caldera (Table 1).

Insight into this problem is provided by the processes that form Mn and Fe oxi-hydroxide zones in hydrothermal conduits from Matupi Harbor (sample H18-21). The pipe was formed in sediments via the concentric deposition of layers of nontronite and Fe oxi-hydroxide, then Mn oxi-hydroxide, and finally a very thin layer of Ca carbonate (Fig. 2b). The Fe- and Mn-enriched layers could develop according to the succession of their oxidation reactions during the mixing of cooling acidic and reduced hydrothermal fluid with oxidized alkaline seawater. The successive deposition of layers testifies to the fading of the hydrothermal activity, because the deposition of Fe(III) oxi-hydroxide and nontronite precedes the deposition of Mn oxi-hydroxide. Trace elements could be borrowed only from this cooling fluid but not from the infinitely large reservoir of seawater, as is the case when oxi-hydroxides are deposits on the seafloor. The Mn oxi-hydroxides are unordered todorokite and asbolane-buserite, as is typical of hydrothermal source of material [22, 62, and others]. Although sample H18-21(1) contains 4.35% Mn, an analogy can be drawn between it and sample B30-72-10 if trace elements are compared in sample H18-21(2), which is enriched in Mn relative to Fe-richer sample H18-21(1). It can be seen in column

C6/C7 in Tables 4 and 5 that the zone of Mn oxi-hydroxides is enriched in Ni > Tl > Co > Mo > Ba > U > Cd. An analogous succession, excluding Cu and Zn (as those are controlled by possible variations in the contents of major elements in hydrothermal fluids, see above), for sample B30-72-10 from the area of the Macauly submarine caldera is Co > Mo > Ni > Cd > Tl > Ba > U. Uranium enrichment in the Mn zone of sample H18-21(1) can be explained by an elevated concentration of this element in the hydrothermal fluid, whereas sample B30-72-10 is practically not enriched in U. Thus, in spite of the differences in the extent of enrichment, the samples are maximally enriched in elements whose oxidation state can change together with Mn (Co and Tl) or those accumulated by sorption from seawater and then accommodated in the structures of Mn minerals.

CONCLUSIONS

Our studies of the chemistry and mineralogy of Fe–Mn deposits in the western part of the Pacific Ocean led us to conclude that these deposits in island arcs are initially formed via the cementing of volcanic–terrigenous material by Fe and Mn oxi-hydroxides of hydrothermal genesis. Fe can be partly derived (in the form of oxi-hydroxides) via the process of halmyrolysis (reactions of volcanic glass with seawater). The deposition of this stage is characterized by very low concentrations of rare and trace elements, and the REE complex is inherited from the volcanic material. Our samples from the Esmeralda submarine volcano demonstrate that the oxi-hydroxide cement evolves from having only Fe oxi-hydroxides in the vicinity of the volcano to having Mn minerals at distances from it. Typically hydrogenic Fe–Mn crusts were found at a distance of 20 km from the volcano, a fact illustrating the local variability of hydrothermal material fluxes.

The differentiation of Mn and Fe in the hydrothermal process was identified in studying the walls of a mineralized-fluid feeder from Matupi Harbor, New Britain Island. The fading of the hydrothermal process is associated with the compositional evolution of the deposits from intercalating nontronite + Fe oxi-hydroxides to zones enriched in Mn oxi-hydroxides in the inner part of the feeder.

The fading of the hydrothermal activity and, as a consequence, an increase in the role of the hydrogenic source of material resulted in changes in the chemistry and mineralogy of crusts B1-14 (from the area of the Smith Pinnacles in the Nampo island arc) and B30-27 (in the Colville Ridge, Kermadec island arc). The compositional variations in the crusts were at a maximum in their Fe constituent, resulting in an increase in the concentrations of trace elements related to Fe oxi-hydroxides: Th, REE, and Y, with REE relatively enriched in Ce and LREE. The Mn component of the crusts is characterized by a significant increase in the concentrations of Co, Ni, Cu, Zn, Mo, W, and Tl.

The closely intergrown aggregates of Fe and Mn oxi-hydroxides typical of hydrogenic crusts are associated with an increase in the concentrations of trace elements belonging to both the Mn group (Co, Ni, Tl, and Mo) and the Fe group (REE, Y, and Th). The accumulation of Mn oxi-hydroxides alone is associated with the enrichment of Co (2587 ppm) and other trace elements related to Mn, in the absolute absence of hydrogenic Fe oxi-hydroxides, as was first discovered in crust B30-72-10 from Macauly Seamount in the Kermadec island arc.

ACKNOWLEDGMENTS

The authors thank A.V. Sivtsov (Institute of the Geology of Ore Deposits, Petrography, Mineralogy, and Geochemistry, Russian Academy of Sciences), L.G. Kashintsev (Shirshov Institute of Oceanology, Russian Academy of Sciences), and K.V. Bryantsev (Moscow State University) for help in preparing material for analysis and in identifying the mineralogical composition of the samples.

This study was supported by the Russian Foundation for Basic Research (project nos. 05-05-65102, 06-05-96002, 06-05-96129, 07-05-00519) and the Program of Fundamental Research of the Presidium of the Russian Academy of Sciences (project 17.3.5).

REFERENCES

1. M. D. Rudnicki and H. Elderfield, "A Chemical Model of the Buoyant Plume above the TAG Vent Field, 26 Degrees N, Mid-Atlantic Ridge," Geochim. Cosmochim. Acta **57**, 2939–2957 (1993).
2. W. Stumm and J. J. Morgan, *Aquatic Chemistry* (John Wiley and Sons, New York, 1981).
3. F. T. Manheim and C. M. Lane-Bostwick, "Cobalt in Ferromanganese Crusts as a Monitor of Hydrothermal Discharge on the Pacific Sea Floor," Nature **335**, 59–62 (1988).
4. A. V. Dubinin, "Inductively Coupled Plasma–Mass-Spectrometry: Determination of Rare Earth Elements in Standard Samples of Oceanic Bottom Deposits," Geokhimiya, No. 11, 1605–1619 (1993).
5. S. V. Strekopytov and A. V. Dubinin, "Determination of Zr, Hf, Mo, W, and Th in Standard Reference Samples of Ocean Sediments by Inductively Coupled Plasma Mass Spectrometry," Zh. Analit. Khim. **52**, 1296–1298 (1997) [J. Analyt. Chem. **52**, 1171–1174 (1997)].
6. I. I. Volkov, "Metal Sources of Present-Day Iron–Manganese Ore Formation in the Oceanic Pelagial. Communication 1. Manganese," Litol. Polezn. Iskop., No. 3, 17–40 (1993).
7. B. G. Lutts, *Geochemistry of Oceanic and Continental Magmatism* (Nedra, Moscow, 1980) [in Russian].
8. S. M. Straub, "Multiple Sources of Quaternary Tephra Layers in the Mariana Trough," J. Volcanol. Geotherm. Res. **76**, 251–276 (1997).
9. J. R. Hein, A. Koschinsky, M. Bau, et al., "Cobalt-Rich Ferromanaganese Crusts in the Pacific," in *Handbook of Marine Mineral Deposits*, Ed. by D. S. Cronan (CRC

Press, Boca Raton, London, New York, 2000), pp. 239–279.

10. A. V. Dubinin, *Rare-Earth Geochemistry in the Ocean* (Nauka, Moscow, 2006) [in Russian].
11. E. Bonatti, T. Kraemer, and H. Rydell, "Classification and genesis of submarine iron-manganese deposits," in *Ferromanganese Deposits of the Ocean Floor*, Ed. by D. Horn (NSF, Washington, 1972), pp. 149–165.
12. I. I. Volkov and A. V. Dubinin, "Rare-Earth Elements in the Hydrothermal Accumulation of Iron and Manganese in the Ocean," Litol. Polezn. Iskop., No. 6, 40–56 (1987).
13. G. M. Gavrilenko, *Submarine Volcanic and Hydrothermal Activity as a Source of Metals in Island-Arc Iron–Manganese Formations* (Dal'nauka, Vladivostok, 1997) [in Russian].
14. G. P. Glasby, G. A. Cherkashov, G. M. Gavrilenko, et al., "Submarine Hydrothermal Activity and Mineralization on the Kurile and Western Aleutian Island Arcs, N.W. Pacific," Mar. Geol **231**, 163–180 (2006).
15. A. P. Sazonov and G. M. Gavrilenko, "Lithological–Geochemical Studies in the Kraternaya Bay (Ushishir Volcano, Kurile Islands)," Vulkanol. Seismol., Nos. 4-5, 48–60 (1994).
16. A. A. Migdisov, Yu. A. Balashov, I. V. Sharkov, et al., "Rare-Earth Element Abundances in Major Lithological Rock Types of the Sedimentary Cover of the Russian Platform," Geokhimiya, No. 6, 789–803 (1994).
17. S. M. DeBari, B. Taylor, K. Spencer, and K. Fujioka, "A Trapped Philippine Sea Origin for MORB from the Inner Slope of the Izu-Bonin Trench," Earth Planet. Sci. Lett. **174**, 183–197 (1999).
18. T. Yu. Uspenskaya and N. S. Skornyakova, *Structure and Texture of Oceanic Ferromanganese Nodules and Crusts* (Nauka, Moscow, 1991) [in Russian].
19. H. Kuno, *Catalogue of the Active Volcanoes of the World Including Solfatara Fields. Part 11. Japan, Taiwan and Marianas* (Intern. Ass. Volcanol, Roma, 1962).
20. I. I. Gushchenko, *Volcanic Eruptions of the World. Catalogue* (Nauka, Moscow, 1979) [in Russian].
21. T. Simkin and L. Siebert, *Volcanoes of the World* (Geoscience Press, Tusson, 1994).
22. T. Yu. Uspenskaya, A. I. Gorshkov, G. M. Gavrilenko, and A. V. Sivtsov, "Ferromanganese Crusts and Nodules of the Kurile Island Arc: Their Structure, Composition, and Genesis," Litol. Polezn. Iskop., No. 4, 30–40 (1989).
23. J. Ostwald, "Some Observations on Todorokites from Marine and Terrestrial Environments," Mineral. Mag. **46**, 253–256 (1982).
24. V. A. Rashidov, A. P. Gorshkov, and A. N. Ivanenko, "Magnetic Studies over Esmeralda and Sofu Submarine Volcanoes," in *Electromagnetic Study of the Deep Structure of the Earth Crust and Upper Mantle on the Sea and Ocean Areas* (IZMIRAN, Moscow, 1981), pp. 213–218 [in Russian].
25. V. A. Rashidov and E. A. Sapozhnikov, "Geological–Geophysical Studies of the Sofu Submarine Volcanic Group, Izu–Bonin Island Arc," Vulkanol. Seismol., No. 4, 39–47 (2001).
26. M. Yasa, F. Murakami, E. Saito, and K. Watanabe, "Submarine Topography of Seamounts on the Volcanic Front of the Izu–Ogasavara (Bonin) Arc," Bull. Geol. Surv. Japan **12**, 703– 743 (1991).
27. *Pilot Chart of Islands of the Northern Pacific Ocean* (MO SSSR, GUNIO, 1975) [in Russian].
28. G. Brown and B. Taylor, "Sea-Floor Mapping of the Sumisu Rift, Izu–Ogasawara (Bonin) Island Arc," Bull. Geol. Surv. Japan **39**, 23–38 (1988).
29. T. Yamazaki, "Heat Flow in the Izu–Ogasawara (Bonin)–Mariana Arc," Bull. Geol. Surv. Japan **43**, 207–235 (1992).
30. T. Yamazaki, T. Ishihara, and F. Murakami, "Magnetic Anomalies over the Izu–Ogasawara (Bonin) Arc, Mariana Arc and Mariana Trough," Bull. Geol. Serv. Japan **42**, 655–689 (1991).
31. M. Yasa, "Sofugan Tectonic Line. A New Tectonic Boundary Separating Northern and Southern Parts of the Ogasawara (Bonin) Arc, Northwest Pacific," in *Formation of Active Ocean Margins*, Ed. by N. Nasu et al. (TERRAPUB, Tokyo, 1985).
32. M. Yasa and M. Nochara, "Petrographic and Geochemical Along-Arc Variations of Volcanic Rocks on the Volcanic Front of the Izu–Ogasawara (Bonin) Arc," Bull. Geol. Surv. Japan **43**, 421–456 (1992).
33. R. Tayama, "Geomorphology, Geology and Coral Reefs of the North Marianas Group," Inst. Geol. Paleontol., Tohoku Imp. Univ. **23** (1936).
34. H. Tanakadate, "Volcanoes in the Mariana Islands in the Japanese Mandated South Seas," Bull. Volcanalogique Ser. 2, **6**, 199–226 (1940).
35. H. H. Hees, "Major Structural Features of the Western North Pacific: An Interpretation of H.O. 5484, Batimetric Chart, Korea to New Guinea," Geo-Mar. Lett. **5**, 417–446 (1948).
36. G. M. Gavrilenko, "Esmeralda Submarine Volcano and Related Iron–Manganese Ore Formation," Vulkanol. Seismol., No. 1, 51–55 (1981).
37. G. M. Gavrilenko, A. P. Gorshkov, and K. A. Skripko, "Activation of Gas–Hydrothermal Activity of Esmeralda Submarine Volcano in January, 1978 and Its Effect on the Chemical Composition of Marine Water," Vulkanol. Seismol., No. 2, 19–29 (1980).
38. A. P. Gorshkov, V. A. Abramov, E. A. Sapozhnikov, et al., "Geological Structure of Esmeralda Submarine Volcano," Vulkanol. Seismol., No. 4, 65–78 (1980).
39. A. P. Gorshkov, G. M. Gavrilenko, N. I. Seliverstov, and K. A. Scripko, "Geologic Structure and Fumarolic Activity of the Esmeralda Submarine Volcano," in *Proceedings of Symposium on Activity of Oceanic Voclanoes, Arquipelago, 1982* (Univ. dos Azores, Ponta Delgada), pp. 271–298 (1982).
40. N. I. Seliverstov, *Seismoacoustic Studies of Transition Zones* (Nauka, Moscow, 1987) [in Russian].
41. Yu. A. Bogdanov, O. G. Sorokhtin, L. P. Zonenshain, et al., *Ferromanganese Crusts and Nodules of Pacific Seamounts* (Nauka, Moscow, 1990) [in Russian].
42. A. V. Dubinin and T. Yu. Uspenskaya, "Geochemistry and Specific Features of Manganese Ore Formation in Sediments of Oceanic Bioproductive Zones," Litol. Polezn. Iskop., No. 1, 1–16 (2006) [Lithol. Mineral. Resour. **41**, 1–14 (2006)].

43. J. Ferguson and I. B. Lambert, "Volcanic Exhalations and Metal Enrichments at Matupi Harbor, New Britain, T.P.N.G.," Econ. Geol. **67**, 25–37 (1972).
44. V. M. Shul'kin, E. V. Tsukanova, and A. B. Maiboroda, "Influence of Recent Hydrothermal Activity on the Distribution of Metals in the Matupi Harbor Waters, Papua—New Guinea," Geokhimiya, No. 3, 389–399 (1992).
45. V. M. Shul'kin, E. V. Tsukanova, and A. B. Maiboroda, "Influence of Recent Hydrothermal Activity on the Metal Content in Bottom Sediments of Matupi Bay: New Britain Islands, Papua–New Guinea," Litol. Polezn. Iskop., No. 2, 3–13 (1992).
46. A. Koschinsky and J. R. Hein, "Uptake of Elements from Seawater by Ferromanganese Crusts: Solid-Phase Associations and Seawater Speciation," Mar. Geol. **198**, 331–351 (2003).
47. I. C. Wright, C. E. J. de Ronde, K. Faure, and J. A. Gamble, "Discovery of Hydrothermal Sulfide Mineralization from Southern Kermadec Arc Volcanoes (SW Pacific)," Earth Planet. Sci. Lett. **164**, 335–343 (1998).
48. C. E. J. de Ronde, E. T. Baker, G. J. Massoth, et al., "Intra-Oceanic Subduction-Related Hydrothermal Venting, Kermadec Volcanic Arc, New Zealand," Earth Planet. Sci. Lett. **193**, 359–369 (2001).
49. Yu. M. Puzankov and Yu. M. Stefanov, "Radioactive Elements as Indicators of the Types of Crust Forming at the Base and Framing of Active Margins," in *Proceedings of 4th International Conference on Processes in Subduction Zones of the Japan, Kurile–Kamchatka, and Aleutian Island Arcs. Correlation between Tectonics, Seismicity, Magma Formation and Eruptions in Volcanic Arcs, Petropavlovsk-Kamchatskii, Russia, 2004*, Ed. by E. I. Gordeev (IVIS DVO RAN, Petropavlovsk-Kamchatskii, 2004) [in Russian].
50. E. F. Lloyd, S. Nathan, I. E. M. Smith, and R. B. Stewart, "Volcanic History of Macauley Island, Kermadec Ridge, New Zealand," New Zealand J. Geol. Geophys. **39**, 295–308 (1996).
51. N. M. Strakhov, *Geochemical Problems of Modern Oceanic Lithogenesis* (Nauka, Moscow, 1976) [in Russian].
52. A. Koschinsky and P. Halbach, "Sequential Leaching of Marine Ferromanganese Precipitates: Genetic Implications," Geochim. Cosmochim. Acta **59**, 5113–5127 (1995).
53. R. Chester and M. J. Hughes, "A Chemical Technique for the Separation of Ferromanganese Minerals, Carbonate Minerals and Adsorbed Trace Elements from Pelagic Sediments," Chem. Geol. **2**, 249–262 (1967).
54. A. V. Dubinin, "Ferromanganese Crust on Pelagic Sediments: Geochemistry and Formation Conditions," Geokhimiya, No. 11, 1152–1163 (1998) [Geochem. Int. **36**, 1041–1051 (1998)].
55. V. N. Lukashin and A. P. Lisitsyn, "Gallium," in *Geochemistry of Hydrolyzate Elements*, Ed. by A. B. Ronov (Nauka, Moscow, 1980) [in Russian].
56. A. R. Flegal and S. Sanudo-Wilhelmy, "Particulate Thallium Fluxes in the Northeast Pacific," Mar. Chem. **28**, 61–75 (1989).
57. J. W. Moffett, "Microbially Mediated Cerium Oxidation in Sea Water," Nature **345**, 421–423 (1990).
58. J. W. Moffett and J. Ho, "Oxidation of Cobalt and Manganese in Sea Water via a Common Microbially Catalyzed Pathway," Geochim. Cosmochim. Acta **60**, 3415–3424 (1996).
59. Y. Takahashi, A. Manceau, N. Geoffroy, et al., "Chemical and Structural Control of the Partitioning of Co, Ce and Pb in Marine Ferromanganese Oxides," Geochim. Cosmochim. Acta **71**, 984–1008 (2007).
60. M. Frank, R. K. O'Nions, J. R. Hein, and V. K. Banakar, "60 Myr Records of Major Elements and Pb–Nd Isotopes from Hydrogenous Ferromanganese Crust: Reconstruction of Seawater Paleochemistry," Geochim. Cosmochim. Acta **63**, 1689–1708 (1999).
61. M. Bau, "Controls on the Fractionation of Isovalent Trace Elements in Magmatic and Aqueous Systems: Evidence from Y/Ho, Zr/Hf, and Lanthanide Tetrad Effect," Contrib. Mineral. Petrol. **123**, 323–333 (1996).
62. T. Kuhn, B. C. Bostick, A. Koschinsky, et al., "Enrichment of Mo Precipitates: Possible Mo Sources, Formation Process and Phase Associations," Chem. Geol. **199**, 29–43 (2003).
63. D. Cronan, *Underwater Minerals* (Academic Press, London, 1980; Moscow: Mir, 1982).